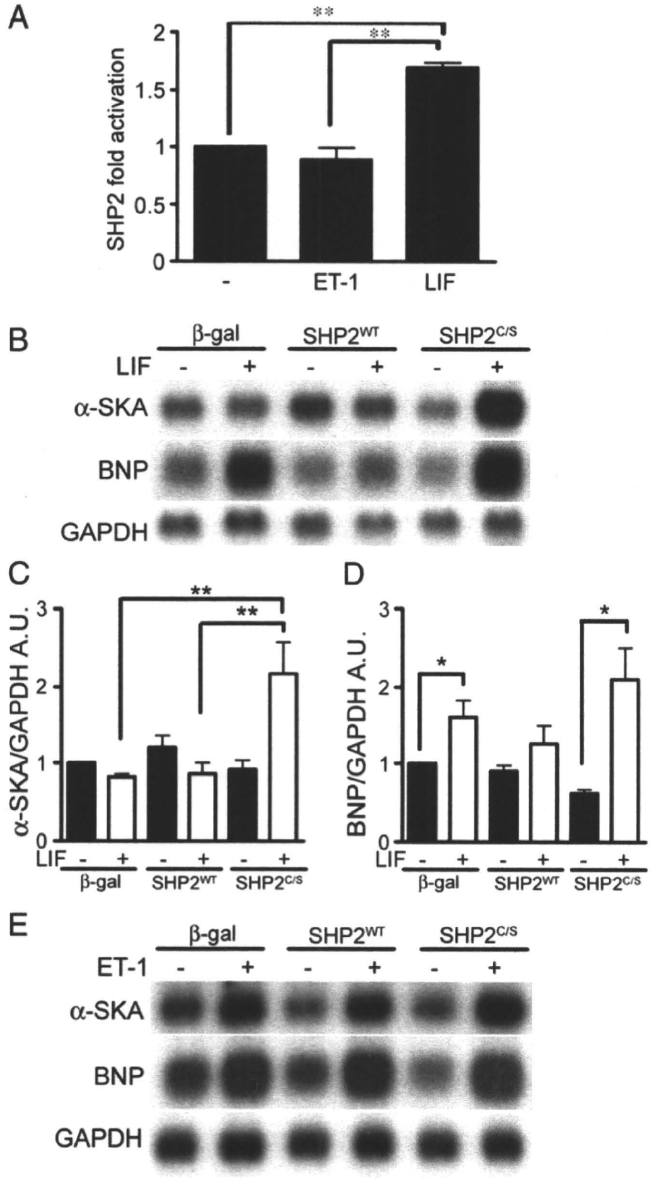

Fig. 4. SHP2 is specifically involved in negative regulation of *α-SKA* gene downstream of LIF–gp130 signaling. (A) Cardiomyocytes were stimulated with vehicle (−), LIF or ET-1 for 5 min. To measure the SHP2 activity, *in vitro* phosphatase assay was performed using anti-SHP2 immunoprecipitates from the corresponding cell lysates as described under "Materials and methods". The results were expressed as fold activation over cells treated with vehicle (−). Values are shown as means ± SEM for three separate myocyte preparation. (**$P \leq 0.01$ by one-way ANOVA.) (B) Cardiomyocytes were infected with adenovirus vectors expressing β-gal, SHP2^{WT}, or SHP2$^{C/S}$ at an m.o.i. of 20 for 8 h and serum-starved. At 24 h after infection, cells were treated with or without LIF for an additional 24 h. Total RNA was isolated and subjected to northern blot analysis using α-SKA and BNP cDNA probes. Equal loading was verified by GAPDH hybridization. (C and D) Relative intensity of the bands for α-SKA (C) or BNP (D) was assessed as the ratio to the intensity of GAPDH. The results were expressed as relative intensity over cells overexpressing β-gal without LIF stimulation. Values are shown as means ± SEM for three separate myocyte preparation. **$P<0.01$ vs AdSHP2$^{C/S}$ LIF (+); *$P<0.05$ vs LIF (−), ($n=3$). A.U., arbitrary unit(s). (E) Cardiomyocytes were infected with adenovirus vectors expressing β-gal, SHP2^{WT}, or SHP2$^{C/S}$ as in (B). Cells were treated with or without ET-1 for 24 h. Total RNA was isolated and subjected to northern blot analysis as in (B). SHP2 was not involved in ET-1-dependent gene regulation of both *α-SKA* and *BNP*.

or SHP2$^{C/S}$ (Fig. 4D). In addition, ET-1 also upregulated *BNP* mRNA almost similarly in those overexpressing β-gal, SHP2^{WT}, or SHP2$^{C/S}$ (Fig. 4E). These data suggest that SHP2 is specifically engaged in negative regulation of *α-SKA* gene downstream of LIF–gp130 signaling.

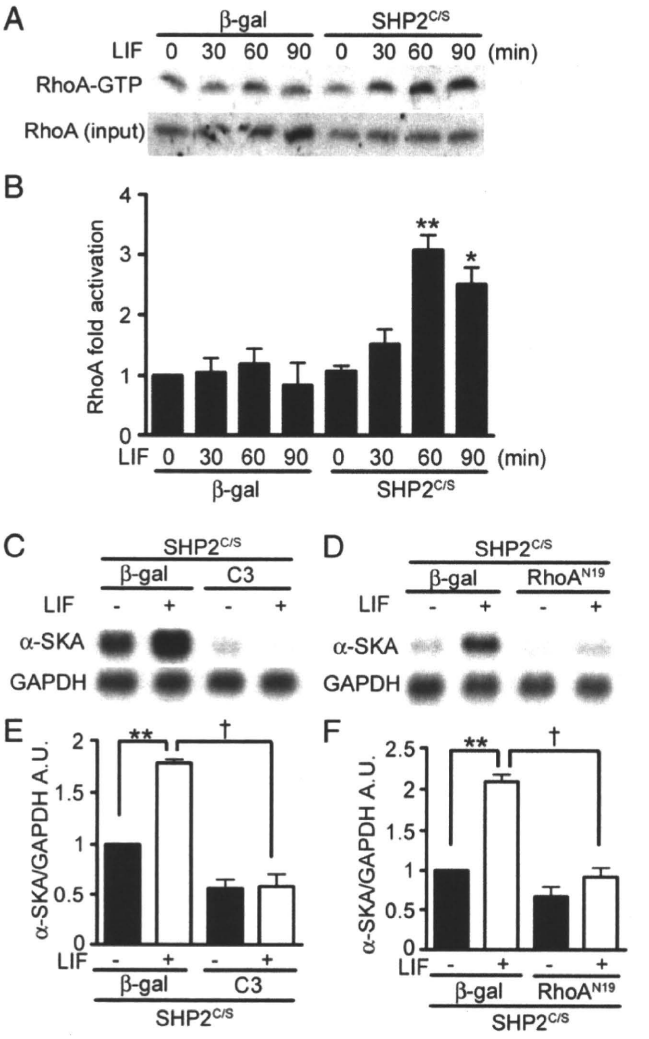

Fig. 5. SHP2 negatively regulates *α-SKA* gene expression via inhibition of RhoA signaling pathway downstream of LIF–gp130 signaling pathway. (A) RhoA was activated upon stimulation with LIF in the cardiomyocytes overexpressing SHP2$^{C/S}$, but not in those overexpressing β-gal. Cardiomyocytes infected with adenovirus vectors expressing β-gal or SHP2$^{C/S}$, were treated with LIF for the indicated time. RhoA-GTP levels were determined almost similarly as described in Fig. 2A. RhoA was activated in those overexpressing SHP2$^{C/S}$, but not in those expressing β-gal. (B) RhoA-GTP was quantified by scanning densitometry and was expressed relative to total RhoA. The results were expressed as relative intensity over cells overexpressing β-gal without LIF stimulation. Values are shown as means ± SEM for three separate myocyte preparation. (**$P<0.01$, by one-way ANOVA). (C and D) Cardiomyocytes were subjected to dual infection of adenovirus vectors expressing either β-gal, C3, or RhoA^{N19} with SHP2$^{C/S}$ at an m.o.i. of 10, respectively. At 24 h after infection, cells were treated with or without LIF for an additional 24 h. Total RNA was isolated and subjected to northern blot analysis (10 μg per each lane) almost similarly as described in Fig. 5A. Co-overexpression of either C3 or RhoA^{N19} almost abrogated the effect of SHP2$^{C/S}$ on *α-SKA* induction. (E and F) Relative intensity of the band for α-SKA was assessed as the ratio to the intensity of GAPDH. The results were expressed as relative intensity over cells co-overexpressing β-gal and SHP2$^{C/S}$ without LIF stimulation. Values are shown as means ± SEM for three separate myocyte preparation. **$P<0.01$ vs LIF (−); †$P<0.01$ vs Adβ-gal ($n=3$). A.U., arbitrary unit(s).

3.4. SHP2 negatively regulates α-SKA gene expression via inhibition of RhoA signaling pathway

Several groups have reported that SHP2 negatively regulates RhoA activity to date [14,16,29]. Therefore, we examined whether SHP2 negatively regulates *α-SKA* gene expression via inhibition of RhoA. Serum-starved cardiomyocytes were infected with adenovirus vectors expressing β-gal or SHP2$^{C/S}$, and treated with LIF. Cell lysates were subjected to pull-down assay to detect the GTP-bound RhoA. In cardiomyocytes overexpressing SHP2$^{C/S}$, the activation of RhoA was

detected from 60 to 90 min after stimulation with LIF, but not in those overexpressing β-gal, indicating that SHP2 might have the inhibitory role for RhoA activation downstream of LIF–gp130 (Figs. 5A and B). In addition, we examined the effect of overexpression of Gab1$^{\Delta SHP2}$, which cannot bind with SHP2, on the RhoA activation in response to LIF. In cardiomyocytes overexpressing Gab1$^{\Delta SHP2}$, the activation of RhoA was detected at 60 min after stimulation with LIF, but not in those overexpressing β-gal, suggesting that SHP2 might exert the inhibitory effect on RhoA through association with Gab1 in response to LIF (Supplemental Fig. S1).

To corroborate the relevance of RhoA activation to *α-SKA* gene upregulation, cells were subjected to dual infection of adenovirus vectors expressing either β-gal, C3, or RhoA^{N19} with SHP2$^{C/S}$. LIF-induced upregulation of *α-SKA* in the myocytes overexpressing SHP2$^{C/S}$ was significantly repressed in those co-expressing C3 or RhoA^{N19} compared with those co-expressing β-gal (Figs. 5C–F). These data suggest that SHP2 negatively regulates *α-SKA* gene expression via inhibition of RhoA.

3.5. SHP2 is required for activation of ERK5 in response to LIF in cardiomyocytes

It has been reported that LIF induces longitudinal elongation of cardiomyocytes through activation of ERK5 [7,32]. Therefore, we examined the activation of ERK5 in the myocytes overexpressing β-gal, SHP2^{WT}, or SHP2$^{C/S}$. LIF induced activation of ERK5 in cardiomyocytes overexpressing β-gal or SHP2^{WT}, but not in those overexpressing

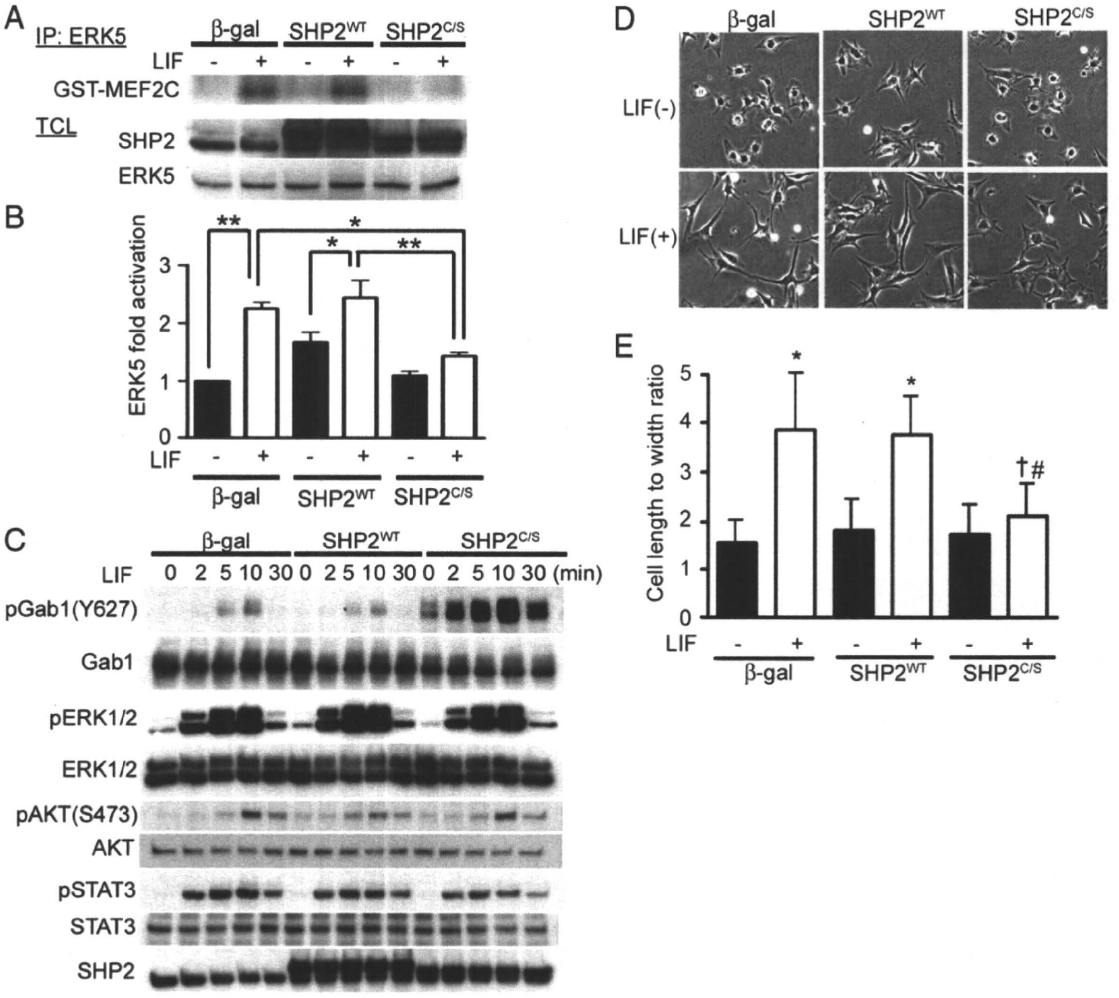

Fig. 6. SHP2 is required for activation of ERK5 and cardiomyocyte elongation after stimulation with LIF. (A) Overexpression of dominant-negative SHP2 abrogated LIF-induced ERK5 activation in cardiomyocytes. Cardiomyocytes, infected with adenovirus vectors expressing β-gal, SHP2^{WT}, or SHP2$^{C/S}$, were stimulated with vehicle (−) or LIF for 15 min. To measure the ERK5 activity, *in vitro* kinase assay was performed using anti-ERK5 immunoprecipitates from the corresponding cell lysates as described under "Materials and methods". ^{32}P-labeled substrates are shown at the top panel (GST-MEF2C). In parallel, cell lysates were subjected to immunoblotting with anti-SHP2 (middle panel) and anti-ERK5 (lower panel) antibodies, to confirm the overexpression of SHP2 and the equal amount loading for *in vitro* kinase assay, respectively. (B) ERK5 activity was quantified by scanning densitometry and was expressed relative to input ERK5 (total cell lysate). The results were expressed as relative intensity over cells overexpressing β-gal treated with vehicle. Values are shown as means ± SEM for three separate myocyte preparation. (**P<0.01, *P<0.05 by one-way ANOVA.) (C) Overexpression of either wild-type or dominant-negative SHP2 does not significantly affect activation of ERK1/2, AKT or STAT3 upon stimulation with LIF in cardiomyocytes. Cardiomyocytes infected with adenovirus vectors expressing β-gal, SHP2^{WT}, or SHP2$^{C/S}$, were treated with LIF for the time indicated. Cell lysates were subjected to western blotting analysis with antibodies indicated at the left. Tyrosine-phosphorylation of Gab1 is enhanced in the cardiomyocytes overexpressing SHP2C/S, compared with those overexpressing β-gal or SHP2^{WT}. Experiments were repeated 3 times with similar results. (D) SHP2 mediates the longitudinal elongation of cardiomyocytes in response to LIF. Cardiomyocytes purified by Percoll gradient method were infected with adenovirus vectors expressing β-gal, SHP2^{WT}, or SHP2$^{C/S}$ at an m.o.i. of 20 for 8 h and serum-starved. At 24 h after infection, cells were treated with vehicle or with LIF for an additional 24 h before fixation. Representative data are shown. (E) A total of 150 cardiomyocytes were examined for the measurement of cell size. For each cardiomyocyte examined, cell length to width ratio was calculated. Values are shown as means ± SEM; *P<0.01 vs LIF (−); †P<0.01 vs Adβ-gal; #P<0.01 vs AdSHP2^{WT}. Experiments were repeated 3 times with similar results.

$SHP2^{C/S}$ (Figs. 6A and B). We examined the other intracellular signaling pathways downstream of gp130. We could not detect the significant difference in the phosphorylation of ERK1/2, AKT, and STAT3 among these cells (Fig. 6C). These data suggest that the phosphatase activity of SHP2 is specifically required for activation of ERK5 in response to LIF in cardiomyocytes.

We previously reported that the complex formation of Gab1 with SHP2 plays a critical role in gp130-dependent longitudinal elongation of cardiomyocytes through activation of ERK5 [7]. Thus, we examined the morphological effects of overexpression of either $SHP2^{WT}$ or $SHP2^{C/S}$ on cardiomyocyte elongation in response to LIF. LIF induced longitudinal elongation of cardiomyocytes in cells overexpressing β-gal or $SHP2^{WT}$. On the contrary, in the myocytes overexpressing $SHP2^{C/S}$, this morphological change was significantly inhibited (Figs. 6D and E). These findings suggest that SHP2 positively regulates longitudinal elongation of cardiomyocytes through activation of ERK5 in response to LIF. Taken together, SHP2 might regulate gp130-dependent cardiomyocyte hypertrophy through both negative effect on the *α-SKA* gene expression and positive effect on the ERK5 activation (Fig. 7).

4. Discussion

The present study revealed that ET-1, but not LIF, induced RhoA activation, accompanied by *α-SKA* gene upregulation in cardiomyocytes. We demonstrated that SHP2 negatively regulates *α-SKA* gene expression through inhibition of RhoA downstream of gp130 in cardiomyocytes. These results are consistent with our previous results showing that Gab1–SHP2 complex negatively regulates *α-SKA* gene expression after stimulation with LIF [7]. In addition, we found that SHP2 is also involved in longitudinal elongation of cardiomyocytes via ERK5 activation in response to LIF.

ET-1 induces *α-SKA* gene upregulation via RhoA in cardiomyocytes (Figs. 2 and 3). Our results coincide with the previous report that RhoA regulates both *α-SKA* gene promoter activity and skeletal muscle differentiation through activation of transcriptional factor SRF [17]. In addition, the changes in cell size, protein production, gene transcription, and myofibril organization induced by ET-1 stimulation are blocked by C3-toxin, Rho-kinase inhibitor, or overexpression of dominant-negative RhoA ($RhoA^{N19}$) [33,34]. Taken together, these findings suggest that RhoA plays a critical role for both cardiomyocyte hypertrophy and *α-SKA* gene upregulation in response to ET-1 (Fig. 7A).

SHP2 negatively regulates RhoA activity in response to LIF in cardiomyocytes. Consistent with our data, the inverse correlation between SHP2 and RhoA activity has been reported in several other cells [14–16]. SHP2 mutant fibroblasts display enhanced stress fiber formation and focal adhesions presumably ascribed to increased RhoA activity [16]. In Mardin–Darby canine kidney (MDCK) cells, overexpression of $SHP2^{C/S}$ markedly increased the formation of stress fibers and focal adhesions presumably through inactivation of RhoA [15]. Similarly, increased expression of SHP2 is prerequisite for nitric oxide-induced cell motility through inactivation of RhoA in differentiated aortic smooth muscle cells [14]. Intriguingly, Kontaridis et al. have recently reported that cardiomyocyte-specific SHP2 knockout mice shows hyperactivation of the RhoA in the myocardium [29], although the activators of SHP2 have not been fully clarified. In this study, we demonstrated that LIF–gp130 signaling induces activation of SHP2, which leads to RhoA inactivation in cardiomyocytes (Fig. 7B). Since it was reported that *α-SKA* gene expression is specifically increased in the human diseased hearts such as left ventricular hypertrophy or valvular disease [5], the roles of SHP2 in *α-SKA* gene regulation in the clinical setting should be addressed in future studies.

SHP2 regulates activation of ERK5 in response to LIF (Figs. 6A and B). In the present study, we confirmed that SHP2 is indeed activated after stimulation with LIF, but not with ET-1 in cardiomyocytes. It was reported that phosphatase activity of SHP2 is required for activation of ERK5 after stimulation of various RTKs such as platelet-derived growth factor receptor and nerve growth factor receptor TrkA [35,36]. We previously reported that Gab1–SHP2 complex formation is prerequisite for LIF-induced activation of ERK5 [7]. SHP2 becomes activated through a conformational change induced by binding of the SH2 domains of SHP2 to phosphorylated tyrosine residues on docking proteins such as Gab family proteins [13]. It has been reported that ERK5 is central to LIF-induced longitudinal elongation of cardiomyocytes [7,32]. Taken together, these findings suggest that LIF induces activation of SHP2 through complex formation of SHP2 with Gab1, leading to longitudinal elongation of cardiomyocytes via ERK5 activation (Fig. 7).

In summary, SHP2 negatively regulates *α-SKA* gene expression through RhoA inactivation and positively regulates elongation of cardiomyocytes through ERK5 activation downstream of gp130 (Fig. 7).

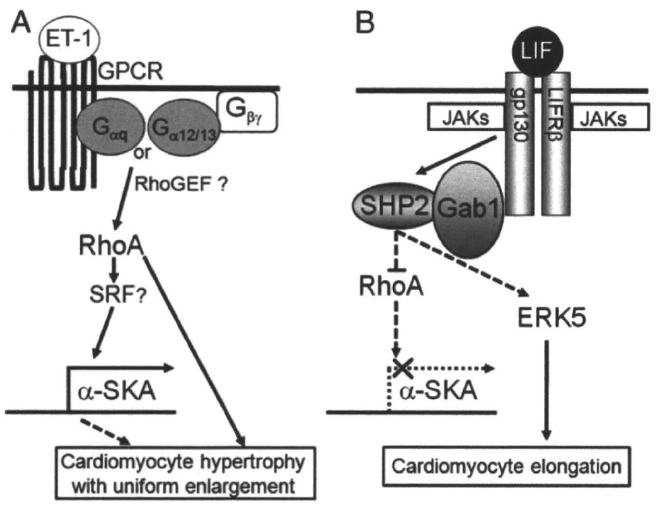

Fig. 7. Schematic illustrations of the roles of SHP2 in the cardiomyocyte elongation downstream of gp130. (A) ET-1 stimulation induces activation of RhoA through $G_{\alpha q}$ or $G_{\alpha q12/13}$. The activation of RhoA induces *α-SKA* gene upregulation presumably through SRF. Importantly, SHP2 is not involved in the ET-1-dependent cardiomyocyte hypertrophy with uniform enlargement of cell size. (B) LIF stimulation induces tyrosine-phosphorylation of both SHP2 and Gab1 through gp130/LIF receptor α (LIFRβ) heterodimer. Complex formation of SHP2 with Gab1 leads to activation of SHP2 and negatively regulates *α-SKA* gene expression through RhoA inactivation. Activation of SHP2 is also required for activation of ERK5 and longitudinal elongation of cardiomyocytes.

Acknowledgments

We thank Masako Suto for her secretary work and also thank Natsuko Maruyama and Manami Sone for their technical assistance. We also thank Dr. Hitoshi Kurose (Kyusyu University) for providing the adenovirus vector expressing C3 and $RhoA^{N19}$, Dr. K. R. Chien (Massachusetts General Hospital, MA, USA) for providing the Northern blot probes for α-SKA, BNP, and GAPDH, and Dr. Motohiko Sato (Yokohama City University) for helpful comments.

This work was supported in part by grants from the Ministry of Education, Science, Sports and Culture of Japan (to Y. N., K. Y-T. and N. M); Japan Heart Foundation Young Investigator's Research Grant (to Y. N.); Suzuken Memorial Foundation (to Y. N.); Astellas Foundation for Research on Metabolic Disorders (to Y.N.); Senri Life Science Foundation (to Y.N.); Miyata Cardiology Research Promotion Funds (to Y.N.); Takeda Medical Research Foundation (to Y.N.); and the Mochida Memorial Foundation for Medical and Pharmaceutical Research (to Y.N.).

Appendix A. Supplementary data

Supplementary data associated with this article can be found, in the online version, at doi:10.1016/j.yjmcc.2010.03.001.

References

[1] Opie LH, Commerford PJ, Gersh BJ, Pfeffer MA. Lancet 2006;367:356–67.
[2] Calderone A, Takahashi N, Izzo Jr NJ, Thaik CM, Colucci WS. Circulation 1995;92: 2385–90.
[3] Vandekerckhove J, Bugaisky G, Buckingham M. J Biol Chem 1986;261:1838–43.
[4] Hewett TE, Grupp IL, Grupp G, Robbins J. Circ Res 1994;74:740–6.
[5] Suurmeijer AJ, Clement S, Francesconi A, Bocchi L, Angelini A, Van Veldhuisen DJ, et al. J Pathol 2003;199:387–97.
[6] MacLellan WR, Schneider MD. Annu Rev Physiol 2000;62:289–319.
[7] Nakaoka Y, Nishida K, Fujio Y, Izumi M, Terai K, Oshima Y, et al. Circ Res 2003;93:221–9.
[8] Wollert KC, Taga T, Saito M, Narazaki M, Kishimoto T, Glembotski CC, et al. J Biol Chem 1996;271:9535–45.
[9] Aoki H, Izumo S, Sadoshima J. Circ Res 1998;82:666–76.
[10] Bishopric NH, Simpson PC, Ordahl CP. J Clin Invest 1987;80:1194–9.
[11] Clement S, Pellieux C, Chaponnier C, Pedrazzini T, Gabbiani G. Differentiation 2001;69:66–74.
[12] Knowlton KU, Michel MC, Itani M, Shubeita HE, Ishihara K, Brown JH, et al. J Biol Chem 1993;268:15374–80.
[13] Neel BG, Gu H, Pao L. Trends Biochem Sci 2003;28:284–93.
[14] Chang Y, Ceacareanu B, Dixit M, Sreejayan N, Hassid A. Circ Res 2002;91:390–7.
[15] Kodama A, Matozaki T, Fukuhara A, Kikyo M, Ichihashi M, Takai Y. Mol Biol Cell 2000;11:2565–75.
[16] Schoenwaelder SM, Petch LA, Williamson D, Shen R, Feng GS, Burridge K. Curr Biol 2000;10:1523–6.
[17] Wei L, Zhou W, Croissant JD, Johansen FE, Prywes R, Balasubramanyam A, et al. J Biol Chem 1998;273:30287–94.
[18] Koyama T, Nakaoka Y, Fujio Y, Hirota H, Nishida K, Sugiyama S, et al. J Biol Chem 2008;283:24234–44.
[19] Maruyama Y, Nishida M, Sugimoto Y, Tanabe S, Turner JH, Kozasa T, et al. Circ Res 2002;91:961–9.
[20] Nakaoka Y, Nishida K, Narimatsu M, Kamiya A, Minami T, Sawa H, et al. J Clin Invest 2007;117:1771–81.
[21] Reid T, Furuyashiki T, Ishizaki T, Watanabe G, Watanabe N, Fujisawa K, et al. J Biol Chem 1996;271:13556–60.
[22] Ogita H, Kunimoto S, Kamioka Y, Sawa H, Masuda M, Mochizuki N. Circ Res 2003;93:23–31.
[23] Fukuhara S, Marinissen MJ, Chiariello M, Gutkind JS. J Biol Chem 2000;275:21730–6.
[24] Nakagawa O, Ogawa Y, Itoh H, Suga S, Komatsu Y, Kishimoto I, Nishino K, et al. J Clin Invest 1995;96:1280–7.
[25] Brown JH, Del Re DP, Sussman MA. Circ Res 2006;98:730–42.
[26] Clerk A, Sugden PH. Circ Res 2000;86:1019–23.
[27] Clerk A, Pham FH, Fuller SJ, Sahai E, Aktories K, Marais R, et al. Mol Cell Biol 2001;21:1173–84.
[28] Kodama A, Matozaki T, Shinohara M, Fukuhara A, Tachibana K, Ichihashi M, et al. Genes Cells 2001;6:869–76.
[29] Kontaridis MI, Yang W, Bence KK, Cullen D, Wang B, Bodyak N, et al. Circulation 2008;117:1423–35.
[30] Wei L, Zhou W, Wang L, Schwartz RJ. AmJPhysiol Heart CircPhysiol 2000;278: H1736–43.
[31] Wei L, Wang L, Carson JA, Agan JE, Imanaka-Yoshida K, Schwartz RJ. FASEB J 2001;15:785–96.
[32] Nicol RL, Frey N, Pearson G, Cobb M, Richardson J, Olson EN. EMBO J 2001;20: 2757–67.
[33] Charron F, Tsimiklis G, Arcand M, Robitaille L, Liang Q, Molkentin JD, et al. Genes Dev 2001;15:2702–19.
[34] Kuwahara K, Saito Y, Nakagawa O, Kishimoto I, Harada M, Ogawa E, et al. FEBS Lett 1999;452:314–8.
[35] Izawa Y, Yoshizumi M, Ishizawa K, Fujita Y, Kondo S, Kagami S, et al. Hypertens Res 2007;30:1107–17.
[36] Rosario M, Franke R, Bednarski C, Birchmeier W. J Cell Biol 2007;178:503–16.

Ca^{2+}/Calmodulin-Dependent Kinase IIδ Causes Heart Failure by Accumulation of p53 in Dilated Cardiomyopathy

Haruhiro Toko, MD, PhD; Hidehisa Takahashi, MD, PhD; Yosuke Kayama, MD; Toru Oka, MD, PhD; Tohru Minamino, MD, PhD; Sho Okada, MD, PhD; Sachio Morimoto, PhD; Dong-Yun Zhan, PhD; Fumio Terasaki, MD, PhD; Mark E. Anderson, MD, PhD; Masashi Inoue, MD, PhD; Atsushi Yao, MD, PhD; Ryozo Nagai, MD, PhD; Yasushi Kitaura, MD, PhD; Toshiyuki Sasaguri, MD, PhD; Issei Komuro, MD, PhD

Background—Dilated cardiomyopathy (DCM), characterized by dilatation and dysfunction of the left ventricle, is an important cause of heart failure. Many mutations in various genes, including cytoskeletal protein genes and contractile protein genes, have been identified in DCM patients, but the mechanisms of how such mutations lead to DCM remain unknown.

Methods and Results—We established the mouse model of DCM by expressing a mutated cardiac α-actin gene, which has been reported in patients with DCM, in the heart (mActin-Tg). mActin-Tg mice showed gradual dilatation and dysfunction of the left ventricle, resulting in death by heart failure. The number of apoptotic cardiomyocytes and protein levels of p53 were increased in the hearts of mActin-Tg mice. Overexpression of Bcl-2 or downregulation of p53 decreased the number of apoptotic cardiomyocytes and improved cardiac function. This mouse model showed a decrease in myofilament calcium sensitivity and activation of calcium/calmodulin-dependent kinase IIδ (CaMKIIδ). The inhibition of CaMKIIδ prevented the increase in p53 and apoptotic cardiomyocytes and ameliorated cardiac function.

Conclusion—CaMKIIδ plays a critical role in the development of heart failure in part by accumulation of p53 and induction of cardiomyocyte apoptosis in the DCM mouse model. (***Circulation.*** **2010;122:891-899.)**

Key Words: apoptosis ■ CaMKII ■ cardiomyopathy ■ heart failure ■ genes, p53

Heart failure is an important cause of morbidity and mortality in many industrial countries, and dilated cardiomyopathy (DCM) is one of its major causes.[1] Although treatments for heart failure have been progressed well in both pharmacological and nonpharmacological aspects, mortality of DCM patients remains high, and the only treatment for DCM patients with severe symptoms is heart transplantation. Because the number of hearts for transplantation is limited, the development of novel therapies for DCM has been awaited.

Clinical Perspective on p 899

DCM, characterized by dilatation and impaired contraction of the left ventricle, is a multifactorial disease that includes both hereditary and acquired forms. The acquired forms of DCM are caused by various factors.[2] Twenty percent to 35% of patients have hereditary forms,[1] and advances in molecular genetic studies during the last decade have revealed many mutations of various genes in DCM patients.[3–5]

Several hypotheses have been reported on the mechanisms of how gene mutations lead to DCM phenotypes. Mutations in genes encoding cytoskeletal proteins such as desmin and muscle LIM protein might disturb the interaction between the sarcomere and Z disk, resulting in impaired force transmission from the sarcomere to the surrounding syncytium.[4,6] On the other hand, mutations in genes encoding contractile proteins such as α-tropomyosin and cardiac troponin T have been reported to induce the decrease in myofilament calcium (Ca^{2+}) sensitivity.[7] An increase in apoptotic cardiomyocytes and/or destruction of membrane structure by calpain activa-

Received January 6, 2010; accepted July 2, 2010.

From the Department of Cardiovascular Science and Medicine, Chiba University Graduate School of Medicine, Chiba, Japan (H. Toko, H. Takahashi, Y.K., T.O., T.M., S.O., I.K.); Department of Cardiovascular Medicine, Osaka University Graduate School of Medicine, Suita, Japan (T.O., I.K.); Department of Clinical Pharmacology, Kyusyu University Graduate School of Medicine, Fukuoka, Japan (S.M., D.Z., T.S.); Department of Internal Medicine III, Osaka Medical College, Takatsuki, Japan (F.T., Y.K.); Department of Internal Medicine, and Molecular Physiology and Biophysics, Carver College of Medicine, University of Iowa, Iowa City (M.E.A.); and Department of Cardiovascular Medicine, University of Tokyo Graduate School of Medicine, Tokyo, Japan (M.I., A.Y., R.N.).

The online-only Data Supplement is available with this article at http://circ.ahajournals.org/cgi/content/full/CIRCULATIONAHA.109.935296/DC1.

Correspondence to Issei Komuro, MD, PhD, Department of Cardiovascular Medicine, Osaka University Graduate School of Medicine, 2-2 Yamadaoka, Suita 565-0871, Japan. E-mail komuro-tky@umin.ac.jp

Circulation **is available at http://circ.ahajournals.org** **DOI: 10.1161/CIRCULATIONAHA.109.935296**

tion have been reported to play a critical role in mutant gene–induced cardiac dysfunction.[8–10] However, the precise mechanisms remain largely unknown as a result, at least in part, of a lack of good animal models of DCM.

Several animal models of DCM have been reported.[11–13] The *mdx* mouse is a model of Duchenne muscular dystrophy, which has mutations in the dystrophin gene.[11] Unlike humans, *mdx* mice rarely show cardiac abnormality, which has limited the utility of *mdx* mice as a model to examine the pathogenesis of DCM. Although Golden Retriever–based muscular dystrophy dogs show DCM phenotypes,[12] the muscular dystrophy dogs are very difficult to maintain and handle. Although BIO 14.6 hamsters lacking δ-sarcoglycan are a good model of DCM,[13] it is difficult to apply genetic approaches to the hamster. To elucidate the molecular mechanisms of how gene mutations cause DCM, appropriate animal models, particularly mouse models, are necessary. We established here a mouse model of DCM by expressing a mutated cardiac α-actin gene (mActin-Tg), which has been reported in patients with DCM, in the heart.[5] mActin-Tg mice showed gradual dilatation and dysfunction of the left ventricle, resulting in death by heart failure. These phenotypes of mActin-Tg mice were quite similar to those of human DCM. In this study, we examined the underlying mechanisms of how this gene mutation leads to DCM using the new mouse model of DCM.

Methods

Detailed experimental methods are described in the online-only Data Supplement.

Mice

We generated transgenic mice (mActin-Tg) that expressed a mutated cardiac α-actin (R312H) with an HA tag in the heart. This mutation has been reported in patients with DCM.[5] Generation of transgenic mice with cardiac-restricted overexpression of human Bcl-2, AC3-I, or nuclear factor of activated T cell (NFAT)–luciferase has been described previously.[14–16] Heterozygous p53-deficient mice were purchased from The Jackson Laboratory (Bar Harbor, Me).[17] Wild-type littermates served as controls for all studies. KN-93 (10 μmol · kg^{-1} · /d^{-1}) was used to inhibit activation of Ca^{2+}/calmodulin-dependent kinase II (CaMKII). Echocardiography was performed on conscious mice.

Histology

For detection of apoptotic cardiomyocytes, we performed terminal deoxynucleotidyl transferase–mediated dUTP nick-end labeling (TUNEL) staining, along with immunostaining for dystrophin.

Western Blot Analysis

Whole-cell lysates were resolved by SDS-PAGE. Western blot analyses were performed with some antibodies. The intensities of Western blot bands were measured with NIH ImageJ software (National Institutes of Health, Bethesda, Md).

Luciferase Assay

Left ventricles were homogenized in luciferase assay buffer as described previously.[15]

Force Measurements

A small fiber was dissected from the skinned left ventricular papillary muscle, and isometric force was measured as described previously.[7]

RNA Extraction and Quantitative Real-Time Polymerase Chain Reaction Analysis

Quantitative real-time polymerase chain reaction was performed with the LightCycler with the Taqman Universal Probe Library and Light Cycler Master. Relative levels of gene expressions were normalized to the mouse GAPDH expression with the ΔΔCt method.[18]

Statistical Analysis

Data are shown as mean±SEM. Multiple-group comparison was performed by 1-way ANOVA followed by the Bonferroni procedure for comparison of means. The F test was used to assess equal variances before comparison between 2 groups. Then, comparisons between 2 groups were performed with the Student t test (when $P>0.05$ in the F test) and the Welch t test (when $P<0.05$ in the F test). Survival rates were analyzed with the log-rank test. Values of $P<0.05$ were considered statistically significant.

Results

DCM Model Mouse

Because there are few useful DCM mouse models, we first generated transgenic mice that expressed a cardiac α-actin R312H mutant with an HA tag under the control of α-myosin heavy chain promoter (mActin-Tg). We obtained 3 independent founders of the transgenic mice (lines 301, 307, and 311). The protein levels of the cardiac α-actin R312H mutant were 1.6-fold in line 301, 3.3-fold in line 307, and 2.2-fold in line 311 compared with those of endogenous cardiac α-actin (Figure IA in the online-only Data Supplement). To confirm the expression of the transgene in cardiomyocytes, we performed immunohistological analyses with antibodies against HA and actinin. The mutated cardiac α-actin protein was colocalized with actinin, suggesting that the cardiac α-actin R312H mutant is incorporated into myofilaments (Figure IB in the online-only Data Supplement). Cardiac systolic function was decreased in mActin-Tg mice at 10 months of age, and the reduction was well correlated with protein levels of the cardiac α-actin R312H mutant (Figure IC in the online-only Data Supplement). To further investigate whether cardiac expression of the cardiac α-actin R312H mutant led to heart failure, we examined another transgenic mouse that expressed cardiac α-actin A331P mutant with an HA tag in the heart. This mutant has been reported to cause hypertrophic cardiomyopathy in human.[19] We obtained 2 independent founders of the transgenic mice that expressed almost the same levels of the cardiac α-actin A331P mutant protein. Although the protein levels of the mutant in the A331P mutant transgenic mice were almost same as those of the R312H mutant in line 307, which had the highest expression (Figure II in the online-only Data Supplement), echocardiography revealed that there were no significant differences in cardiac systolic function, wall thickness, and left ventricular dimension between cardiac α-actin A331P mutant transgenic mice and their wild-type littermates (Table I in the online-only Data Supplement). Although it is not known at present why the expression of cardiac α-actin A331P mutant did not induce hypertrophic cardiomyopathy, these results suggest that cardiac dysfunction of mActin-Tg mice is due to cardiac expression of the cardiac α-actin R312H mutant in the heart, not to high-level expression of the cardiac α-actin protein with the tag (lines 307 and 311).

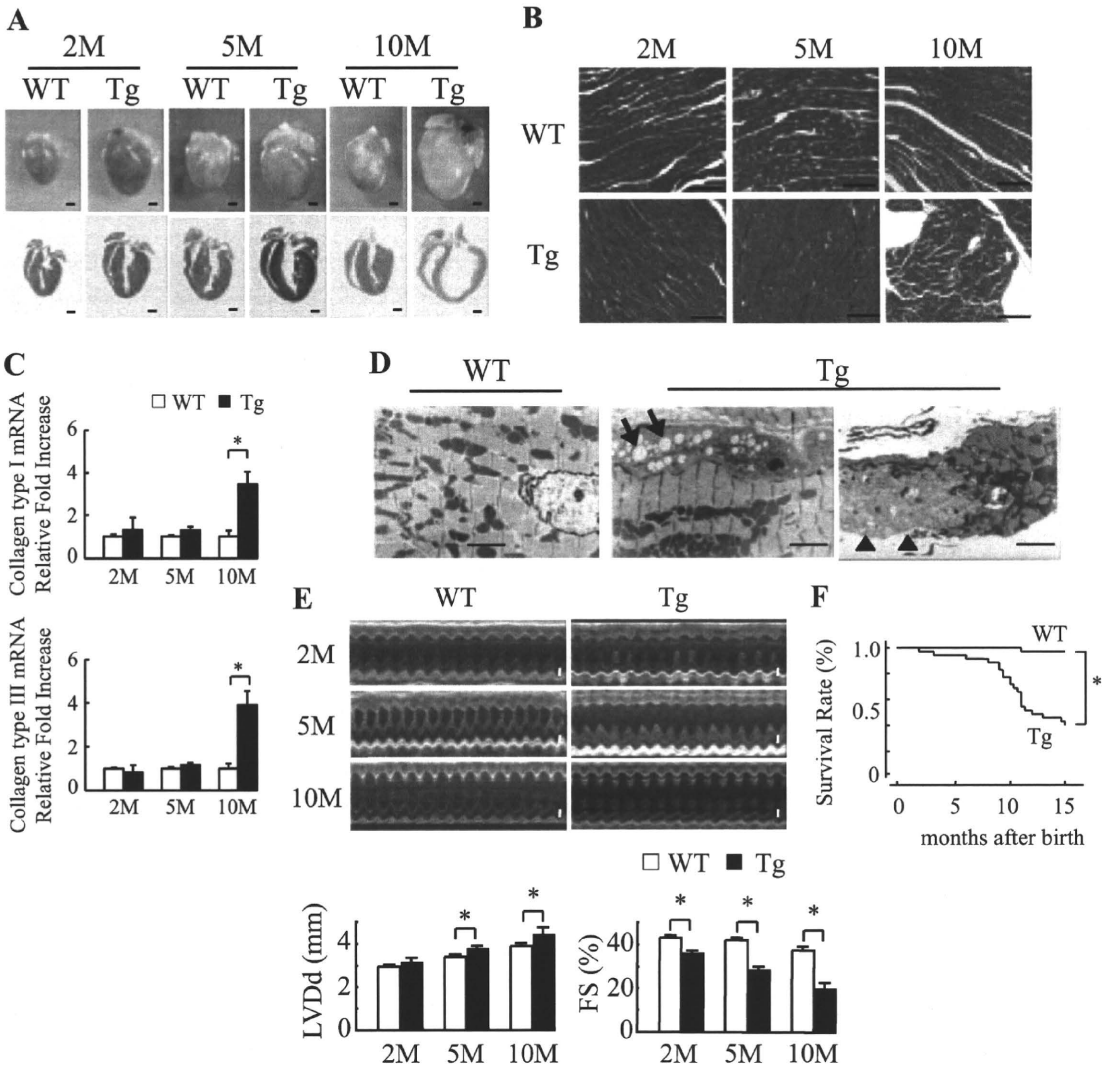

Figure 1. Mutated cardiac α-actin R312H transgenic mice. A, Gross morphology (top) and sections (bottom) of wild-type littermates (WT) or mActin-Tg (Tg) hearts at 2, 5, and 10 months (M) of age. Scale bar=1 mm. B, Masson trichrome staining. Scale bar=100 μm. C, Relative levels of collagen types I and III in hearts were normalized to GAPDH expression. *$P<0.05$ vs WT mice. n=4 in each group. D, Electron microscopic analyses. Cytoplasmic vacuolization (arrow) and lysis of myofibrils (arrowhead) were detected in the hearts of Tg mice. Scale bar=10 μm. E, Echocardiographic analysis. Scale bar=1 mm. LVDd indicates left ventricular end-diastolic dimension; FS, fractional shortening. *$P<0.05$. F, Kaplan-Meier survival curve. *$P<0.05$ vs WT mice. WT, n=32; Tg, n=37.

We used line 307, which expressed the cardiac α-actin R312H mutant at the highest levels, for further studies. The hearts in mActin-Tg mice were larger than those of wild-type littermates (Figure 1A), and heart weight and the ratio of heart weight to body weight were much increased in mActin-Tg mice (Table II in the online-only Data Supplement). Marked cardiac fibrosis was observed in mActin-Tg mice at 10 months of age, with increased expression of collagen types I and III (Figure 1B and 1C). Electron microscopic analyses showed that there were degenerated cardiomyocytes with an increase in vacuolar formation and lysis of myofibrils in mActin-Tg mice (Figure 1D). Echocardiography revealed that left ventricular dimension was gradually increased and that fractional shortening was reduced in mActin-Tg mice compared with wild-type littermates (Table II in the online-only Data Supplement and Figure 1E). The expression levels of ANP and SERCA2a were gradually increased and decreased in mActin-Tg mice, respectively (Figure III in the online-only Data Supplement). There was no significant difference in blood pressure, but heart rate was increased in mActin-Tg mice (Table II in the online-only Data Supplement), suggesting that the sympathetic nervous system is activated. Surface ECG monitoring showed low amplitude of the R wave in mActin-Tg mice (Table II in the online-only Data Supplement), which is often observed in human DCM patients. Many mActin-Tg mice died by 35 weeks of age (Figure 1F). Although telemetric ECG recording did not show life-threatening arrhythmia in mActin-Tg mice (data not shown), spontaneous Ca^{2+} sparks and Ca^{2+} waves were significantly increased in the cardiomyocytes of mActin-Tg mice (Table III in the online-only Data Supplement), suggesting that not only cardiac pump failure but also arrhythmia could be the cause of death. These phenotypes of mActin-Tg mice were quite similar to those of human DCM.

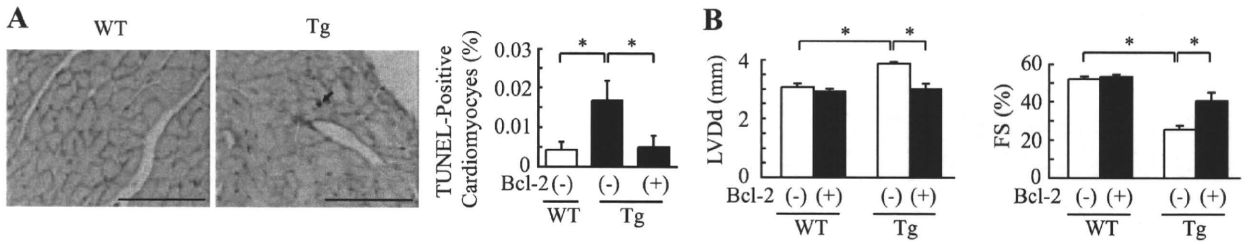

Figure 2. Increase in Bcl-2 preserves cardiac function in mActin-Tg mice. A, Double immunostaining for TUNEL (black) and dystrophin (red) of the heart (left). The graph indicates quantitative analyses of TUNEL-positive cardiomyocytes. Scale bar=100 μm. n=4 in each group. *$P<0.05$. B, Echocardiographic analyses at 5 months of age. *$P<0.05$. WT/Bcl-2(−), n=5; WT/Bcl-2(+), n=10; Tg/Bcl-2(−), n=10; Tg/Bcl-2(+), n=5. WT indicates wild-type littermates; Tg, mActin-Tg mice; LVDd, left ventricular end-diastolic dimension; and FS, fractional shortening.

Apoptotic Cardiomyocytes Are Increased in mActin-Tg Hearts

It has been reported that apoptosis of cardiomyocytes is observed in hearts of human DCM[10] and that cardiomyocyte death might cause cardiac dysfunction.[20] We thus examined apoptosis of cardiomyocytes by TUNEL labeling in left ventricular sections of wild-type littermates and mActin-Tg mice at 5 months of age. The number of TUNEL/dystrophin double-positive cardiomyocytes was significantly larger in mActin-Tg mice compared with wild-type littermates (Figure 2A). To examine whether the increase in apoptotic cardiomyocytes causes cardiac dysfunction in mActin-Tg mice, we generated double-transgenic mice by crossing mActin-Tg mice and the transgenic mice, which overexpress the antiapoptotic protein Bcl-2 in cardiomyocytes [mActin(+)/Bcl-2(+)-DTg].[14] The number of apoptotic cardiomyocytes in mActin(+)/Bcl-2(+)-DTg mice was significantly less compared with mActin-Tg mice (Figure 2A). Echocardiography revealed that the left ventricular dimension was smaller and fractional shortening was better in mActin(+)/Bcl-2(+)-DTg mice than in mActin-Tg mice at 5 months of age (Figure 2B), suggesting that the increase in apoptotic cardiomyocytes causes cardiac dysfunction in the DCM mouse model.

p53 Is Involved in Cardiomyocyte Apoptosis in mActin-Tg Mice

To clarify the mechanisms of how the cardiac α-actin R312H mutant induces apoptosis of cardiomyocytes, we examined expression levels of apoptosis-related proteins by Western blot analyses. The protein levels of p53 and Bax were higher in mActin-Tg mice compared with wild-type littermates (Figure 3A). Several key proapoptotic genes have been reported to be positively regulated by p53,[21] and increased expression of p53 induces left ventricular dilatation and dysfunction in several types of mice.[22,23] To determine the role of p53 in gene mutation–induced DCM, we crossed mActin-Tg mice and heterozygous p53-deficient mice [p53(+/−)]. Because many of homozygous p53-deficient mice [p53(−/−)] died of tumors before 5 months of age,[17] we used heterozygous p53-deficient mice [p53(+/−)] for this study. Echocardiography revealed that left ventricular dimension was smaller and fractional shortening was better in mActin-Tg/p53(+/−) mice than in mActin-Tg/p53(+/+) mice at 5 months of age (Figure 3B). Loss of a single p53 allele attenuated the increase of Bax (Figure 3C) and reduced the number of apoptotic cardiomyocytes in mActin-Tg mice (Figure 3D). These results suggest that p53-induced cardiomyocyte apoptosis induces dilatation and dysfunction of the left ventricle in the DCM mouse model.

Myofilament Calcium Sensitivity Is Decreased and Calcium-Dependent Enzymes Are Activated in mActin-Tg Mice

Many gene mutations associated with DCM have been reported to induce the decrease of myofilament Ca^{2+} sensi-

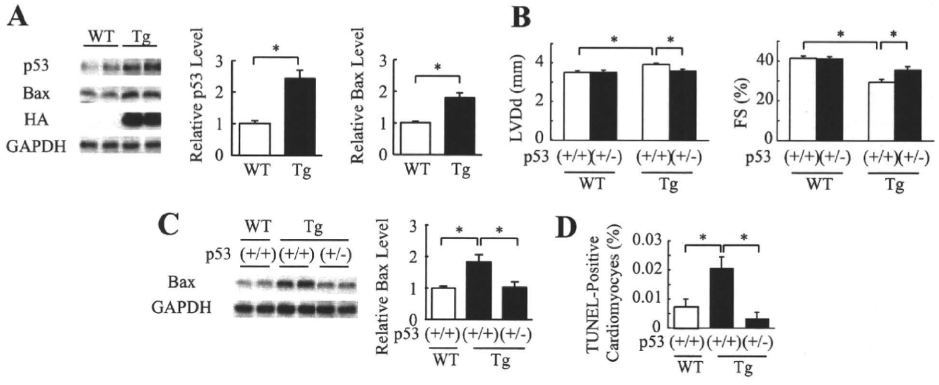

Figure 3. Inhibition of p53 preserves cardiac function in mActin-Tg mice. A, Western blot analyses in the hearts of wild-type littermates (WT) or mActin-Tg (Tg) mice at 5 months of age. The graph indicates relative protein levels of p53 (n=8 in each group) or Bax (n=10 in each group). *$P<0.05$. B, Echocardiographic analyses at 5 months of age. WT/p53(+/+), n=12; WT/p53(+/−), n=10; Tg/p53(+/+), n=19; Tg/p53(+/−), n=14. *$P<0.05$. C, Western blot analyses in the hearts. The graph indicates relative protein levels of Bax. n=6 in each group. *$P<0.05$. D, Quantitative analyses of TUNEL-positive cardiomyocytes. n=5 in each group. *$P<0.05$.

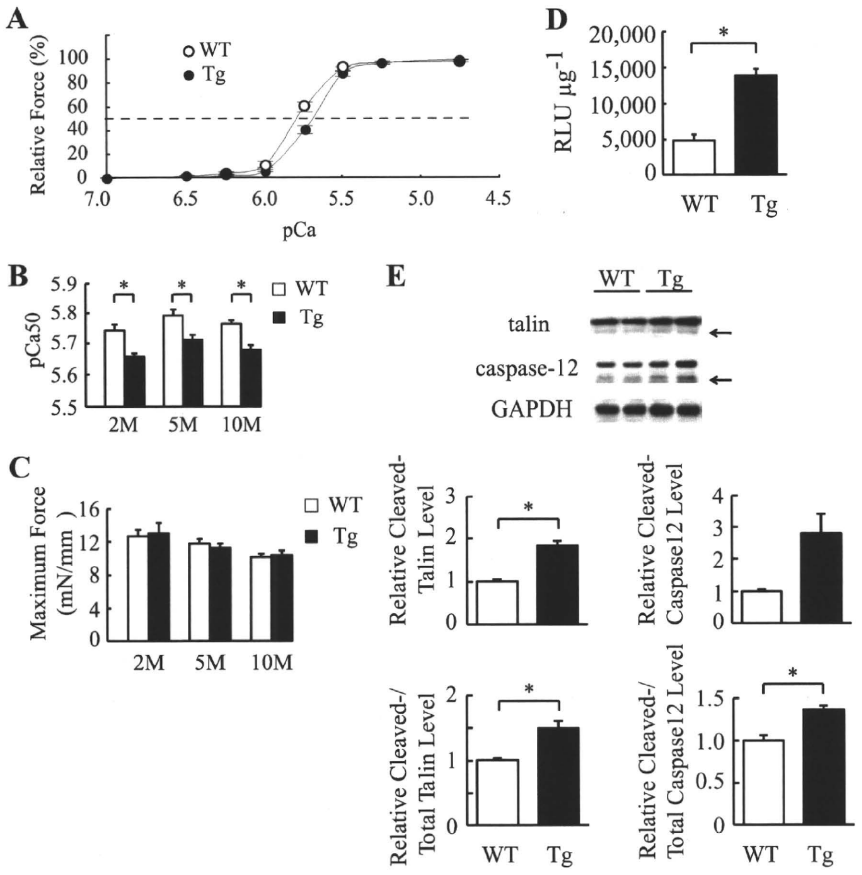

Figure 4. Myofilament Ca^{2+} sensitivity is decreased and Ca^{2+}-dependent enzymes are activated in mActin-Tg mice (Tg). A, Force-pCa relationship in skinned cardiac muscle fiber at 5 months of age. The broken line indicates pCa50. Wild-type (WT; n=11) and Tg (n=10) fibers were prepared from 3 isolated hearts. B, Ca^{2+} sensitivity (pCa50) of force-pCa relationships in skinned cardiac muscle fibers at 2, 5, and 10 months (M) of age. *$P<0.05$. C, Maximum force-generating capabilities. Fibers (n=9 to 11) were prepared from 3 isolated hearts of each group. D, The NFAT–luciferase reporter activity (RLU μg^{-1}) in the hearts at 5 months of age. n=4 in each group. *$P<0.05$. E, Western blot analyses in the hearts. Arrows indicate the calpain cleaved forms of talin and caspase-12. The graph indicates relative protein levels of cleaved talin or caspase-12 and ratio of cleaved forms to total proteins. n=4 in each group. *$P<0.05$.

tivity.[7] We examined myofilament Ca^{2+} sensitivity in mActin-Tg mice. The force-pCa relationship was shifted rightward in mActin-Tg mice compared with wild-type littermates (Figure 4A). The pCa value at half-maximal force generation (pCa50, an index of Ca^{2+} sensitivity) was significantly lower in mActin-Tg mice (Figure 4B), suggesting that skinned cardiac muscle fibers prepared from mActin-Tg mice show a decrease in Ca^{2+} sensitivity of force generation. The degree was the same between 2 and 10 months of age (Figure 4B), suggesting that the reduction in Ca^{2+} sensitivity is not a result of cardiac dysfunction. Despite the reduced Ca^{2+} sensitivity, there was no significant difference in maximum force-generating capabilities between wild-type littermates and mActin-Tg mice (Figure 4C). The decrease in myofilament Ca^{2+} sensitivity is expected to influence intracellular Ca^{2+} handling in cardiomyocytes of mActin-Tg mice. To clarify whether intracellular Ca^{2+} levels in cardiomyocytes are changed in mActin-Tg mice, we examined the activity of Ca^{2+}-dependent enzymes such as calcineurin and calpain. We generated double-transgenic mice by crossing mActin-Tg mice and the transgenic mice carrying a luciferase reporter driven by a cluster of NFAT binding sites, which is activated by calcineurin-dependent NFAT proteins.[15] The NFAT–luciferase reporter activity was higher in mActin-Tg mice than in wild-type littermates at 5 months of age (Table IV in the online-only Data Supplement and Figure 4D). Furthermore, the ratio of the calpain-induced cleaved forms of talin and caspase-12 to total proteins was significantly increased in mActin-Tg mice compared with wild-type littermates (Figure 4E). We next examined Ca^{2+} transients in cardiomyocytes using fluo-3AM (Figure IVA in the online-only Data Supplement). Although the time to peak amplitude of Ca^{2+} was significantly slower in mActin-Tg mice than in wild-type littermates (Figure IVB in the online-only Data Supplement), there was no significant difference in peak amplitude between wild-type littermates and mActin-Tg mice at 2 and 10 months of age (Figure IVC in the online-only Data Supplement). The expression levels of SERCA2a, but not Na^+/Ca^{2+} exchanger, were decreased in mActin-Tg mice (Figure III in the online-only Data Supplement).

CaMKIIδ Is Activated in mActin-Tg Mice

It has been reported that among Ca^{2+}-dependent proteins, expression of CaMKIIδ is increased in human DCM hearts[24] and that overexpression of CaMKIIδ induces heart failure in mice.[25,26] We thus examined the expression and phosphorylation of CaMKIIδ and phosphorylation of its target protein, phospholamban (Thr17). The protein levels of total (both CaMKIIδB and CaMKIIδC) and phosphorylated CaMKIIδ and of phosphorylated phospholamban (Thr17) were increased in mActin-Tg mice compared with wild-type littermates (Figure 5A and Figure VA in the online-only Data Supplement), suggesting that CaMKIIδ is activated in mActin-Tg mice. The protein levels of phosphorylated phospholamban (Ser16), which is activated by protein kinase A, were also increased in mActin-Tg mice (Figure 5A).

Because it has been reported that the sympathetic nervous system is activated in failing hearts and that β-adrenergic

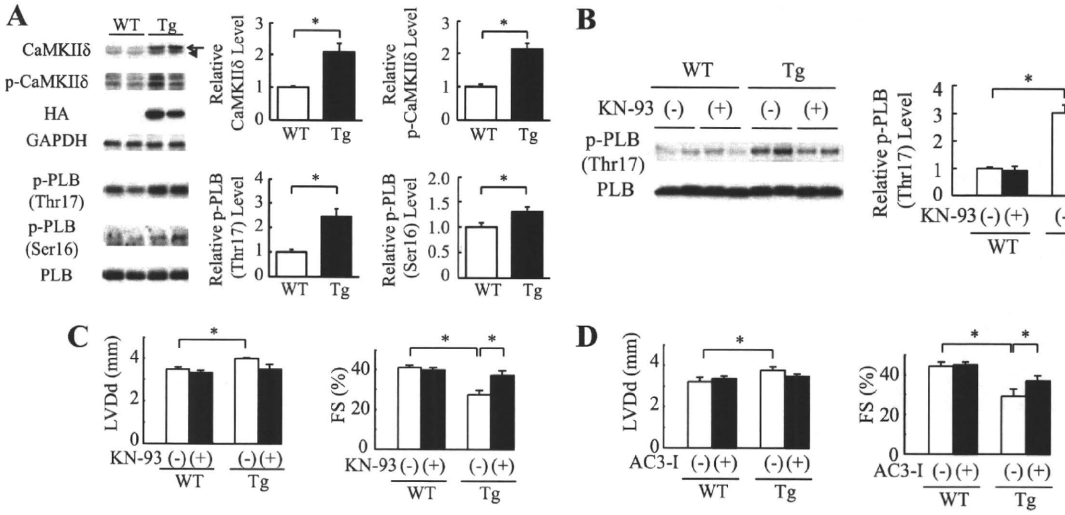

Figure 5. CaMKIIδ is activated in mActin-Tg mice. A, Western blot analyses in the hearts of wild-type littermates (WT) or mActin-Tg (Tg) mice at 5 months of age. The graph indicates relative protein levels of total and phosphorylated CaMKIIδ (p- CaMKIIδ) or phosphorylated phospholamban (p-PLB). Arrow and arrowhead indicate CaMKIIδB and CaMKIIδC, respectively. n=6 in each group. *P<0.05. B, Western blot analyses in the hearts at 5 months of age. The graph indicates relative protein levels of p-PLB (Thr17). n=4 in each group. *P<0.05. C and D, Echocardiographic analyses at 5 months of age. WT/KN-93(−), n=11; WT/KN-93(+), n=7; Tg/KN-93(−), n=8; Tg/KN-93(+), n=6; WT/AC3-I(−), n=8; WT/AC3-I(+), n=18; Tg/AC3-I(−), n=10; Tg/AC3-I(+), n=14. KN indicates KN-93; LVDd, left ventricular end-diastolic dimension; and FS, fractional shortening. *P<0.05.

receptor signal activates CaMKIIδ,[27] we treated mActin-Tg mice with the β-blocker bisoprolol to clarify the relationship between β-adrenergic receptor signal and activation of CaMKIIδ. The treatment with bisoprolol ameliorated cardiac dysfunction of mActin-Tg mice, and there was no significant difference in cardiac function between wild-type littermates and mActin Tg mice with bisoprolol treatment (Figure VB in the online-only Data Supplement). Furthermore, the increase in CaMKIIδ levels in mActin-Tg mice was prevented by bisoprolol treatment (Figure VC in the online-only Data Supplement), suggesting that the activation of CaMKIIδ in mActin-Tg mice might be due to activation of β-adrenergic receptor signaling.

To test whether activation of CaMKIIδ induces cardiac dysfunction, we first treated mActin-Tg mice with KN-93, a CaMKII inhibitor. Levels of both phosphorylated phospholamban (Thr17) and phospholamban (Ser16) were decreased by KN-93 treatment in mActin-Tg mice (Figure 5B and Figure VD in the online-only Data Supplement). Echocardiography revealed that KN-93 treatment prevented left ventricular dilatation and preserved cardiac function in mActin-Tg mice (Figure 5C). On the other hand, KN-92, an inactive derivative of KN-93, did not show any effects (Figure VE in the online-only Data Supplement). To confirm the role of CaMKIIδ in mActin-Tg mice, we crossed mActin-Tg mice and AC3-I mice, which expressed the CaMKII-inhibitory peptide AC3-I in the heart [mActin(+)/AC3-I(+)-DTg].[16] Echocardiography revealed that fractional shortening was better in mActin(+)/AC3-I(+)-DTg mice than in mActin(+)/AC3-I(−)-Tg mice (Figure 5D), suggesting that the activation of CaMKIIδ in the DCM mouse model induces left ventricular dilatation and contractile dysfunction.

We next examined the relation between CaMKIIδ activation and p53. The increase in p53 was attenuated by treatment with KN-93 or overexpression of AC3-I (Figure 6A and Figure VIA in the online-only Data Supplement). Furthermore, KN-93 treatment inhibited the increase in Bax expression and TUNEL-positive cardiomyocytes (Figure 6A and 6B). It has been reported that CaMKIIδC, but not CaMKIIδB, induces cardiomyocyte death.[27–29] To clarify the mechanism of how CaMKIIδ increases protein levels of p53 and which

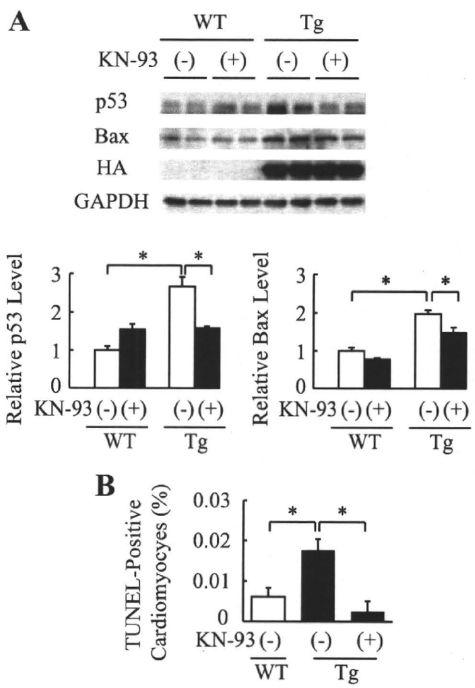

Figure 6. CaMKIIδ regulates expression of p53 in cardiomyocytes. A, Western blot analyses in the hearts of wild-type littermates (WT) or mActin-Tg (Tg) mice. The graph indicates relative protein levels of p53 or Bax. n=4 in each group. *P<0.05. B, Quantitative analyses of TUNEL-positive cardiomyocytes. n=5 in each group. *P<0.05.

CaMKIIδ, δB or δC, plays an important role in apoptosis of cardiomyocytes, we transfected constitutively active forms of CaMKIIδ (caCaMKIIδ) into cardiomyocytes. Only caCaMKIIδC, not caCaMKIIδB, increased protein levels of p53 (Figure VIB in the online-only Data Supplement). Furthermore, p53 protein levels in caCaMKIIδC-transfected cardiomyocytes did not increase with MG132 treatment compared with MOCK-treated cardiomyocytes (Figure VIC in the online-only Data Supplement). These results suggest that activation of CaMKIIδC increases apoptotic cardiomyocytes at least in part via stabilization of p53 in the DCM mouse model.

Discussion

In the present study, we established a novel mouse model of DCM to clarify the mechanisms of how mutant genes lead to DCM (Table II in the online-only Data Supplement and Figure 1). The mice expressing cardiac α-actin R312H mutant in the heart, which has been reported to cause DCM in humans,[5] showed dilatation and dysfunction of left ventricle with an increase in ANP messenger RNA levels, which is consistent with human heart failure (Figure 1A and 1E and Table II and Figure III in the online-only Data Supplement). Higher heart rate and hyperphosphorylated phospholamban (Ser16) (Table II in the online-only Data Supplement and Figure 5A) suggest the activation of the sympathetic nervous system to compensate for reduced cardiac systolic function, resulting in an increase in spontaneous Ca^{2+} sparks and Ca^{2+} waves (Table III in the online-only Data Supplement). Myofilament Ca^{2+} sensitivity was decreased in mActin-Tg mice even at 2 months of age (Figure 4B), when cardiac phenotypes such as left ventricular dilatation and cardiac fibrosis were not recognized (Table II in the online-only Data Supplement and Figure 1). These results suggest that the decrease in myofilament Ca^{2+} sensitivity is a primary cause of, not a secondary result from, cardiac dysfunction. Because these phenotypes were quite similar to those of human DCM, mActin-Tg mice are useful for examining the underlying mechanisms of how gene mutations lead to DCM.

There was no significant difference in the peak amplitude of Ca^{2+} transients between wild-type littermates and mActin-Tg mice (Figure IVC in the online-only Data Supplement), suggesting that global Ca^{2+} levels underlying each contractile cycle do not differ between the 2 groups. It has been reported that the peak amplitude of Ca^{2+} transients, which is associated with decreased Ca^{2+} sensitivity and systolic dysfunction, is higher in another mouse model of DCM, [7] suggesting that Ca^{2+} transients are augmented to compensate for decreased myofilament Ca^{2+} sensitivity in this model. In mActin-Tg mice, despite the preserved Ca^{2+} transients (Figure IVC in the online-only Data Supplement), global cardiac function was gradually impaired (Table II in the online-only Data Supplement). Local Ca^{2+} concentration has been reported to be important for the activation of Ca^{2+}-dependent enzymes such as calcineurin, calpain, and CaMKII in cardiomyocytes.[30] The activation of these molecules in mActin-Tg mice (Figures 4D, 4E, and 5A) might be attributed to an increase in local Ca^{2+} levels. It still remains to be determined whether local Ca^{2+} levels are really increased and, if so, how the decrease in Ca^{2+} sensitivity increases local Ca^{2+} levels.

Recent reports have shown that CaMKIIδ plays a crucial role in cardiovascular diseases.[16,31] The transgenic mice that overexpressed CaMKIIδ showed heart failure with systolic dysfunction and left ventricular dilatation.[25,26] In this study, CaMKIIδ was activated in the hearts of mActin-Tg mice (Figure 5A), and inhibition of CaMKIIδ by KN-93 or AC3-I ameliorated cardiac dysfunction in mActin-Tg mice (Figure 5C and 5D), suggesting that CaMKIIδ also plays an important role in gene mutation–induced cardiac dysfunction.

It has been reported that apoptosis of cardiomyocytes is observed in hearts of human DCM[10] and that cardiomyocyte death could cause cardiac dysfunction.[20] However, it remains unclear whether apoptosis of cardiomyocytes causes cardiac dysfunction and how cardiomyocyte apoptosis is induced in hearts of DCM. In this study, there were more apoptotic cardiomyocytes in mActin-Tg mice (Figure 2A), and cardiac function was improved by protecting cardiomyocytes from apoptosis through overexpression of Bcl-2 (Figure 2B). These results suggest that cardiomyocyte apoptosis plays a crucial role in the development of DCM. Several key proapoptotic and antiapoptotic genes have been reported to be positively or negatively regulated by p53, and increased expression of p53 induces left ventricular dilatation and dysfunction in mice deficient in MDM4, an E3 ligase for p53.[23] Furthermore, we have recently demonstrated that p53 is critically involved in pressure overload–induced cardiac dysfunction.[22] The protein levels of p53 were increased in mActin-Tg mice (Figure 3A), and loss of a single p53 allele reduced the number of apoptotic cardiomyocytes (Figure 3D) and improved cardiac function (Figure 3B). These results suggest that p53 is critically involved in induction of cardiomyocyte apoptosis, resulting in left ventricular dysfunction in the mouse model of DCM.

The present study indicates that p53 might be a therapeutic target for DCM. In this study, CaMKIIδ was activated in the hearts of mActin-Tg mice (Figure 5A), and the inhibition of CaMKIIδ attenuated the increase in p53 protein levels (Figure 6A and Figure VIA in the online-only Data Supplement), suggesting that CaMKIIδ regulates protein levels of p53 in the DCM model mice. Although it remains to be determined how CaMKIIδ regulates protein levels of p53, inhibition of CaMKIIδ may become a new therapeutic strategy for DCM patients by reducing p53 protein levels in the heart.

Limitations

This study has a couple limitations. First, we cannot completely rule out the nonspecific effects of overexpression of cardiac α-actin gene with tag because of a lack of transgenic mice that overexpress wild-type cardiac α-actin gene. However, we think the cardiac dysfunction observed in mActin-Tg was due to cardiac expressions of the cardiac α-actin R312H mutant in the heart, not to high-level expressions of the cardiac α-actin protein with tag because of the following reasons: We obtained 3 independent founders of the transgenic mice, and the reduction in cardiac function was well correlated with protein levels of the cardiac α-actin R312H mutant (Figure I in the online-only Data Supplement). An-

other transgenic mouse that expressed cardiac α-actin A331P mutant with an HA tag in the heart did not show cardiac dysfunction (Table I in the online-only Data Supplement), although the protein levels of the mutant in the A331P mutant transgenic mice were almost same as those of the R312H mutant in line 307, which had the highest expression (Figure II in the online-only Data Supplement). Second, we found that CaMKIIδC increases p53 protein levels mainly by its stabilization, but the underlying mechanisms remain to be determined.

Acknowledgments

We thank J. Robbins (Children's Hospital Research Foundation, Cincinnati, Ohio) for a fragment of α-myosin heavy chain gene promoter, J.D. Molkentin (Children's Hospital Research Foundation, Cincinnati, Ohio) for NFAT-luciferase reporter transgenic mice, M.D. Schneider (Imperial College, London, UK) for Bcl-2 transgenic mice, and E.N. Olson (UT Southwestern Medical Center, Dallas, Tex) for constitutively active forms of CaMKIIδ. We thank E. Fujita, R. Kobayashi, Y. Ishiyama, M. Ikeda, I. Sakamoto, A. Furuyama, and Y. Ohtsuki for technical support, as well as M. Iiyama, K. Matsumoto, Y. Ishikawa, and Y. Yasukawa for animal care.

Sources of Funding

This work was supported by a Grant-in-Aid for Scientific Research on Priority Areas (to Dr Komuro) and a Grant-in-Aid for Scientific Research (C) (20590857 to Dr Oka) from the Ministry of Education, Culture, Sports, Science and Technology; the Japan Heart Foundation/Novartis Grant for Research Award on Molecular and Cellular Cardiology; Japan Foundation for Applied Enzymology; Suzuken Memorial Foundation; and Mitsubishi Pharma Research Foundation (to Dr Toko). This work was supported by National Institutes of Health grants R01 HL079031, R01 HL070250, and R01 HL096652 and by the Fondation Leducq Award to the Alliance for Calmodulin Kinase Signaling in Heart Disease (to Dr Anderson).

Disclosures

Dr Anderson is named on patents claiming to treat heart failure by CaMKII inhibition and is a cofounder of Allosteros. The other authors report no conflicts.

References

1. Michels VV, Moll PP, Miller FA, Tajik AJ, Chu JS, Driscoll DJ, Burnett JC, Rodeheffer RJ, Chesebro JH, Tazelaar HD. The frequency of familial dilated cardiomyopathy in a series of patients with idiopathic dilated cardiomyopathy. *N Engl J Med.* 1992;326:77–82.
2. Maron BJ, Towbin JA, Thiene G, Antzelevitch C, Corrado D, Arnett D, Moss AJ, Seidman CE, Young JB. Contemporary definitions and classification of the cardiomyopathies: an American Heart Association scientific statement from the Council on Clinical Cardiology, Heart Failure and Transplantation Committee; Quality of Care and Outcomes Research and Functional Genomics and Translational Biology Interdisciplinary Working Groups; and Council on Epidemiology and Prevention. *Circulation.* 2006;113:1807–1816.
3. Ahmad F, Seidman JG, Seidman CE. The genetic basis for cardiac remodeling. *Annu Rev Genomics Hum Genet.* 2005;6:185–216.
4. Knoll R, Hoshijima M, Hoffman HM, Person V, Lorenzen-Schmidt I, Bang ML, Hayashi T, Shiga N, Yasukawa H, Schaper W, McKenna W, Yokoyama M, Schork NJ, Omens JH, McCulloch AD, Kimura A, Gregorio CC, Poller W, Schaper J, Schultheiss HP, Chien KR. The cardiac mechanical stretch sensor machinery involves a Z disc complex that is defective in a subset of human dilated cardiomyopathy. *Cell.* 2002;111:943–955.
5. Olson TM, Michels VV, Thibodeau SN, Tai YS, Keating MT. Actin mutations in dilated cardiomyopathy, a heritable form of heart failure. *Science.* 1998;280:750–752.
6. Towbin JA, Bowles NE. Genetic abnormalities responsible for dilated cardiomyopathy. *Curr Cardiol Rep.* 2000;2:475–480.
7. Du CK, Morimoto S, Nishii K, Minakami R, Ohta M, Tadano N, Lu QW, Wang YY, Zhan DY, Mochizuki M, Kita S, Miwa Y, Takahashi-Yanaga F, Iwamoto T, Ohtsuki I, Sasaguri T. Knock-in mouse model of dilated cardiomyopathy caused by troponin mutation. *Circ Res.* 2007;101:185–194.
8. Kawada T, Masui F, Tezuka A, Ebisawa T, Kumagai H, Nakazawa M, Toyo-Oka T. A novel scheme of dystrophin disruption for the progression of advanced heart failure. *Biochim Biophys Acta.* 2005;1751:73–81.
9. Kyoi S, Otani H, Matsuhisa S, Akita Y, Tatsumi K, Enoki C, Fujiwara H, Imamura H, Kamihata H, Iwasaka T. Opposing effect of p38 MAP kinase and JNK inhibitors on the development of heart failure in the cardiomyopathic hamster. *Cardiovasc Res.* 2006;69:888–898.
10. Olivetti G, Abbi R, Quaini F, Kajstura J, Cheng W, Nitahara JA, Quaini E, Di Loreto C, Beltrami CA, Krajewski S, Reed JC, Anversa P. Apoptosis in the failing human heart. *N Engl J Med.* 1997;336:1131–1141.
11. Bulfield G, Siller WG, Wight PA, Moore KJ. X chromosome-linked muscular dystrophy (mdx) in the mouse. *Proc Natl Acad Sci U S A.* 1984;81:1189–1192.
12. Cooper BJ, Winand NJ, Stedman H, Valentine BA, Hoffman EP, Kunkel LM, Scott MO, Fischbeck KH, Kornegay JN, Avery RJ, Williams JR, Schmickel RD, Sylvester JE. The homologue of the Duchenne locus is defective in X-linked muscular dystrophy of dogs. *Nature.* 1988;334:154–156.
13. Nigro V, Okazaki Y, Belsito A, Piluso G, Matsuda Y, Politano L, Nigro G, Ventura C, Abbondanza C, Molinari AM, Acampora D, Nishimura M, Hayashizaki Y, Puca GA. Identification of the Syrian hamster cardiomyopathy gene. *Hum Mol Genet.* 1997;6:601–607.
14. Tanaka M, Nakae S, Terry RD, Mokhtari GK, Gunawan F, Balsam LB, Kaneda H, Kofidis T, Tsao PS, Robbins RC. Cardiomyocyte-specific Bcl-2 overexpression attenuates ischemia-reperfusion injury, immune response during acute rejection, and graft coronary artery disease. *Blood.* 2004;104:3789–3796.
15. Wilkins BJ, Dai YS, Bueno OF, Parsons SA, Xu J, Plank DM, Jones F, Kimball TR, Molkentin JD. Calcineurin/NFAT coupling participates in pathological, but not physiological, cardiac hypertrophy. *Circ Res.* 2004;94:110–118.
16. Zhang R, Khoo MS, Wu Y, Yang Y, Grueter CE, Ni G, Price EE Jr, Thiel W, Guatimosim S, Song LS, Madu EC, Shah AN, Vishnivetskaya TA, Atkinson JB, Gurevich VV, Salama G, Lederer WJ, Colbran RJ, Anderson ME. Calmodulin kinase II inhibition protects against structural heart disease. *Nat Med.* 2005;11:409–417.
17. Donehower LA, Harvey M, Slagle BL, McArthur MJ, Montgomery CA Jr, Butel JS, Bradley A. Mice deficient for p53 are developmentally normal but susceptible to spontaneous tumours. *Nature.* 1992;356:215–221.
18. VanGuilder HD, Vrana KE, Freeman WM. Twenty-five years of quantitative PCR for gene expression analysis. *Biotechniques.* 2008;44:619–626.
19. Olson TM, Doan TP, Kishimoto NY, Whitby FG, Ackerman MJ, Fananapazir L. Inherited and de novo mutations in the cardiac actin gene cause hypertrophic cardiomyopathy. *J Mol Cell Cardiol.* 2000;32:1687–1694.
20. Wencker D, Chandra M, Nguyen K, Miao W, Garantziotis S, Factor SM, Shirani J, Armstrong RC, Kitsis RN. A mechanistic role for cardiac myocyte apoptosis in heart failure. *J Clin Invest.* 2003;111:1497–1504.
21. Ryan KM, Phillips AC, Vousden KH. Regulation and function of the p53 tumor suppressor protein. *Curr Opin Cell Biol.* 2001;13:332–337.
22. Sano M, Minamino T, Toko H, Miyauchi H, Orimo M, Qin Y, Akazawa H, Tateno K, Kayama Y, Harada M, Shimizu I, Asahara T, Hamada H, Tomita S, Molkentin JD, Zou Y, Komuro I. p53-induced inhibition of Hif-1 causes cardiac dysfunction during pressure overload. *Nature.* 2007;446:444–448.
23. Xiong S, Van Pelt CS, Elizondo-Fraire AC, Fernandez-Garcia B, Lozano G. Loss of Mdm4 results in p53-dependent dilated cardiomyopathy. *Circulation.* 2007;115:2925–2930.
24. Hoch B, Meyer R, Hetzer R, Krause EG, Karczewski P. Identification and expression of delta-isoforms of the multifunctional Ca2+/calmodulin-dependent protein kinase in failing and nonfailing human myocardium. *Circ Res.* 1999;84:713–721.
25. Zhang T, Johnson EN, Gu Y, Morissette MR, Sah VP, Gigena MS, Belke DD, Dillmann WH, Rogers TB, Schulman H, Ross J Jr, Brown JH. The cardiac-specific nuclear delta(B) isoform of Ca2+/calmodulin-dependent protein kinase II induces hypertrophy and dilated cardiomyopathy associated with increased protein phosphatase 2A activity. *J Biol Chem.* 2002;277:1261–1267.

26. Zhang T, Maier LS, Dalton ND, Miyamoto S, Ross J Jr, Bers DM, Brown JH. The deltaC isoform of CaMKII is activated in cardiac hypertrophy and induces dilated cardiomyopathy and heart failure. *Circ Res.* 2003;92: 912–919.
27. Zhu WZ, Wang SQ, Chakir K, Yang D, Zhang T, Brown JH, Devic E, Kobilka BK, Cheng H, Xiao RP. Linkage of beta1-adrenergic stimulation to apoptotic heart cell death through protein kinase A-independent activation of Ca2+/calmodulin kinase II. *J Clin Invest.* 2003;111:617–625.
28. Peng W, Zhang Y, Zheng M, Cheng H, Zhu W, Cao CM, Xiao RP Cardioprotection by CaMKII-deltaB is mediated by phosphorylation of heat shock factor 1 and subsequent expression of inducible heat shock protein 70. *Circ Res.* 2010;106:102–110.
29. Zhu W, Woo AY, Yang D, Cheng H, Crow MT, Xiao RP. Activation of CaMKIIdeltaC is a common intermediate of diverse death stimuli-induced heart muscle cell apoptosis. *J Biol Chem.* 2007;282: 10833–10839.
30. Wu X, Zhang T, Bossuyt J, Li X, McKinsey TA, Dedman JR, Olson EN, Chen J, Brown JH, Bers DM. Local InsP3-dependent perinuclear Ca2+ signaling in cardiac myocyte excitation-transcription coupling. *J Clin Invest.* 2006;116:675–682.
31. Ling H, Zhang T, Pereira L, Means CK, Cheng H, Gu Y, Dalton ND, Peterson KL, Chen J, Bers D, Heller Brown J. Requirement for Ca2+/calmodulin-dependent kinase II in the transition from pressure overload-induced cardiac hypertrophy to heart failure in mice. *J Clin Invest.* 2009;119:1230–1240.

CLINICAL PERSPECTIVE

Heart failure is an important cause of morbidity and mortality in many industrial countries, and dilated cardiomyopathy (DCM) is one of its major causes. Molecular genetic studies over the last 2 decades have revealed many mutations of various genes in DCM patients, but the precise mechanisms of how such mutations lead to DCM remain largely unknown partly because of a lack of good animal models of DCM. Here, we established the mouse model of DCM by expressing a mutated cardiac α-actin gene, which has been reported in patients with DCM, in the heart. The transgenic mice showed gradual dilatation and dysfunction of the left ventricle, resulting in death by heart failure. These phenotypes of the transgenic mice were quite similar to those of human DCM. The number of apoptotic cardiomyocytes and protein levels of p53 were increased in the hearts of the DCM mice. Overexpression of Bcl-2, an antiapoptotic factor, or downregulation of p53 decreased the number of apoptotic cardiomyocytes and improved cardiac function. The DCM mice showed activation of CaMKIIδ. The inhibition of CaMKIIδ prevented the increase in p53 and apoptotic cardiomyocytes and ameliorated cardiac function. These results suggest that CaMKIIδ plays a critical role in the development of heart failure in part by accumulation of p53 and induction of cardiomyocyte apoptosis in the DCM mouse model. The inhibition of CaMKIIδ may become a new therapeutic strategy for DCM patients.

Original Article

Molecular Mechanisms of Ezetimibe-Induced Attenuation of Postprandial Hypertriglyceridemia

José C. Sandoval[1], Yumiko Nakagawa-Toyama[2], Daisaku Masuda[1], Yoshihiro Tochino[3], Hajime Nakaoka[1], Ryota Kawase[1], Miyako Yuasa-Kawase[1], Kazuhiro Nakatani[1], Miwako Inagaki[1], Kazumi Tsubakio-Yamamoto[1], Tohru Ohama[1], Akifumi Matsuyama[4], Makoto Nishida[2], Masato Ishigami[5], Issei Komuro[1], and Shizuya Yamashita[1]

[1]Department of Cardiovascular Medicine, Osaka University Graduate School of Medicine, Osaka, Japan
[2]Health Care Center, Osaka University, Osaka, Japan
[3]Department of Metabolic Medicine, Osaka University Graduate School of Medicine, Osaka, Japan
[4]Laboratory for Somatic Stem Cell Therapy, Foundation of Biomedical Research and Innovation, Kobe, Japan
[5]Department of Biomedical Informatics, Division of Health Sciences, Osaka University Graduate School of Medicine, Osaka, Japan

Aim: Postprandial hypertriglyceridemia (PHTG) has been shown repeatedly to be associated with metabolic syndrome and atherosclerotic cardiovascular diseases. We have recently reported that ezetimibe inhibits PHTG in patients with type IIb hyperlipidemia. Ezetimibe was also reported to attenuate PHTG in combination with low-dose statins in patients with obesity or metabolic syndrome. We reported CD36-deficient (CD36KO) mice as a new model for PHTG, in which the synthesis of chylomicron (CM) in the small intestines is enhanced. In the current study, we investigated the effect of ezetimibe on PHTG in this mouse model of metabolic syndrome.

Methods: Wild-type (WT) mice fed a western diet, and CD36KO mice fed a normal chow diet, respectively, were treated for 3 weeks with and without ezetimibe, followed by an evaluation of triglyceride (TG) concentrations by enzymatic method and by high performance liquid chromatography (HPLC) as well as those of and apolipoprotein (Apo) B-48 in plasma and intestinal lymph after oral fat loading with olive oil. Intestinal mucosa was also harvested to evaluate the transcriptional regulation of the genes involved in the intestinal production of ApoB-containing lipoproteins.

Results: Ezetimibe dramatically reduced PHTG in both WT and CD36KO mice. HPLC analysis of plasma showed that the decrease in TG content in CM and CM remnants-sized particles contributed to this suppression, suggesting that CM production in the small intestines might be reduced after ezetimibe treatment. Intestinal lymph was collected after oral fat loading in ezetimibe-treated and non-treated mice. Both TG content and ApoB-48 mass were decreased in ezetimibe-treated mice. The quantitative RT-PCR of intestinal mucosa showed down-regulation of the mRNA expression of FATP4 and ApoB in both groups along with FABP2, DGAT1, DGAT2 and SCD1 in WT mice at postprandial state after ezetimibe treatment.

Conclusion: Ezetimibe alone reduces PHTG by blocking both the absorption of cholesterol and the intracellular trafficking and metabolism of long-chain fatty acids in enterocytes, resulting in the reduction of the formation of ApoB-48 which is necessary for the ApoB48-containing lipoprotein production in the small intestines.

J Atheroscler Thromb, 2010; 17:914-924.

Key words; Postprandial hypertriglyceridemia, Ezetimibe, CD36 deficiency, Long-chain fatty acids, Apolipoprotein B-48

Address for correspondence: Shizuya Yamashita, Department of Cardiovascular Medicine, Osaka University Graduate School of Medicine, 2-2 Yamada-oka, Suita, Osaka 565-0871, Japan
E-mail: shizu@imed2.med.osaka-u.ac.jp
Received: January 6, 2010
Accepted for publication: January 29, 2010

Introduction

Metabolic syndrome (MetS) is defined as a cluster of interrelated factors commonly associated with atherosclerotic cardiovascular diseases: central obesity, modestly high blood pressure, impaired glucose

metabolism and atherogenic dyslipidemia[1], including elevated triglyceride (TG) in the fasting state.

Besides the early hours of the day before breakfast, we are constantly in a non-fasting state. Accumulating evidence concerning nonfasting TG levels as a predictor of cardiovascular diseases[2] and stroke[3] suggest atherosclerosis as a postprandial phenomenon in which intestine-derived TG-rich lipoproteins, such as chylomicron (CM) and CM remnants, would play an important role[4-6], which Zilversmit stated three decades ago[7].

CD36, or fatty acid translocase, is an 88 kD scavenger receptor class B that is expressed in many cells, such as monocytes, macrophages, microvascular endothelial cells, adipocytes, skeletal and cardiac myocytes and enterocytes. It binds multiple ligands, including long-chain fatty acids (FAs) and oxidized low density lipoprotein[8]. Patients with CD36 deficiency present with increased remnant lipoproteins and decreased high density lipoprotein (HDL)-cholesterol, as well as impaired glucose metabolism based upon insulin resistance. All these findings suggest that CD36 deficiency may be considered a monogenic form of MetS[9]. CD36 knockout (CD36KO) mice present with an excessive postprandial plasma TG and FA response after acute oral fat loading compared to wild-type (WT) mice[10]. Previous studies in our laboratory using CD36KO mice reported a postprandial increase in plasma CM and CM remnants with enhanced TG synthesis in the small intestines, suggesting that the main cause of postprandial hypertriglyceridemia (PHTG) in CD36KO mice was the increased *de novo* synthesis of small CM in enterocytes[11]. These findings established CD36KO mice as a model to evaluate PHTG in a MetS environment.

Ezetimibe, a cholesterol absorption inhibitor that acts by blocking the sterol-induced internalization of the key cholesterol transporter, Niemann-Pick C1 Like 1 (NPC1L1), in enterocytes[12] has been demonstrated to lower total and LDL-cholesterol levels significantly in patients with primary and mixed hypercholesterolemia as a coadjuvant therapy to either statins[13] or fibrates[14]. In these studies, ezetimibe was also found to decrease other important atherogenic factors significantly, such as fasting TG and total apolipoprotein B (ApoB) levels in plasma. Moreover, ezetimibe has been demonstrated to reduce PHTG in combination with low-dose statins in patients with obesity and metabolic syndrome comparable to high-dose statins alone[15].

Recently, our group reported that ezetimibe alone significantly reduced PHTG in Japanese subjects with type IIb hyperlipidemia[16], suggesting that ezetimibe might also play a role in regulating the production of TG-rich lipoproteins in addition to act as a cholesterol absorption inhibitor. Since investigations concerning ezetimibe and its mechanism of action on lipid metabolism have primarily focused on sterol metabolism, we prioritized the need to establish molecular mechanisms that participate in the TG-lowering effect of ezetimibe in the postprandial state. For that purpose, we performed oral fat loading in ezetimibe-treated and non-treated wild-type (WT) mice fed a western diet and CD36KO mice fed a chow diet as an animal model of PHTG. We demonstrated that ezetimibe reduces PHTG by decreasing the absorption of both cholesterol and long-chain FAs through enterocytes, which affected intestinal FA transport, TG production, and CM formation in both mice strains.

Materials and Methods

Animals

Male C57BL6/J WT and CD36KO mice created on a C57BL6/J background (kindly provided by Mason. W. Freeman, M.D., Ph.D., Professor of Harvard Medical School)[17], 8–10 weeks of age were used for this experiment. Each mouse strain was separated into two groups in the following manner: CD36KO mice were fed a chow diet (MF; Oriental BioLaboratories, Chiba, Japan) either with or without supplementation of 10 mg/kg ezetimibe (Schering-Plough, USA), and WT mice were fed a western diet either with or without supplementation of 10 mg/kg ezetimibe. The animals were housed in a temperature-controlled environment at 12-hour dark-light cycles with free access to food and water. After 3 weeks of treatment, mice in each group were divided into 2 subgroups. One subgroup was euthanized after fasting for 12 h and the other was fasted for 12 h followed by acute ingestion of 17 μL/g body weight of olive oil (Nacalai Tesque, Kyoto, Japan) by intragastric gavage, and then euthanized 3 h after initiating oral fat loading. Plasma, intestinal lymph and tissues were collected from both subgroups at the time of euthanization. Additionally, WT mice fed a standard chow diet were used as controls for the TG determination study. The experimental protocol was approved by the Ethics Review Committee for Animal Experimentation of Osaka University Graduate School of Medicine (IEXAS).

Lipid Determination and Lipoprotein Analysis of Plasma and Intestinal Lymph

Cholesterol and TG concentrations in plasma and intestinal lymph for each mouse were measured

using an enzymatic method (Wako Pure Chemical Industries, Tokyo, Japan) according to the manufacturer's protocol. Plasma and lymph lipoprotein profiles were analyzed by an online dual enzymatic method using high performance liquid chromatography (HPLC) at Skylight Biotech Inc. (Akita, Japan)[18]. Two hundred microliters of plasma or lymph were dissolved in loading buffer and loaded onto TSK gel Lipopropak XL columns; TG concentrations in the flow-through were measured continuously and simultaneously. The correspondence of the size of lipoprotein fractions (CM, very low density lipoprotein (VLDL), LDL, and HDL-sized fractions) and the elution time were; CM (particle diameter >80 nm, elution time: 15–17 min), VLDL (particle diameter: 30–80 nm, elution time: 17–22 min), LDL (particle diameter: 16–30 nm, elution time: 22–28 min), and HDL (particle diameter: 8–16 nm, elution time: 28–37 min).

Collection of Intestinal Lymph in Postprandial State

Five mice from each group, previously fasted for 12 h, were gavaged with olive oil (17 μL/g body weight). Three hours later, the animals were anesthetized and the intestinal lymphatic trunk was cannulated with a 27-gauge needle connected to a polyethylene tube (PE-50), which was pretreated with EDTA-containing water. The procedure was performed in accordance with the modified method described by Bollman *et al.*[19]. The collected intestinal lymph was used for HPLC and protein detection by western blot.

Determination of Labeled Triolein Absorption

Mice from each group were fasted for 12 h and gavaged with 3 μCi of [9,10-^{3}H(N)] triolein (PerkinElmer, MA, USA) mixed into 17 μL/g body weight of olive oil. Three hours after fat loading, the mice were euthanized and blood samples were collected from the inferior vena cava. The activity of radiolabeled tritium in 250 μL plasma was determined by scintillation counting using a WALLAC Winspectral™ 1414 Liquid Scintillation Counter.

Protein Detection by Western Blot

One microliter of sample (plasma or lymph) was subjected to 4–12% SDS-polyacrylamide gel electrophoresis (SDS-PAGE; TEFCO, Tokyo, Japan), later transferred onto an Immobilon-P transfer membrane (Millipore Co., USA), and blocked by Blocking One (Nacalai Tesque, Kyoto, Japan). The blotted membrane was then incubated with anti-mouse ApoB-48/B-100 antibody (BIODESIGN International, ME, USA) and anti-rabbit IgG as a secondary antibody (NA934V; GE Healthcare Backinghamshire, UK). Bands corresponding to ApoB-48 were detected with the ECL Advance Detection Kit (GE Healthcare, UK).

RNA Extraction, cDNA Synthesis and Quantitative Real-Time PCR

Mice were fasted for 12 h, gavaged with olive oil as previously stated, and their small intestines were removed, flushed with ice-cold phosphate-buffered saline and divided into three sections of equal length; the proximal two-thirds of mucosa were gently scraped and stored in RNAlater RNA stabilization reagent (QIAGEN GmbH, Germany) at −20℃.

Total RNA from tissue samples were extracted and purified using the RNeasy Plus Mini Kit (cat. 74134; QIAGEN GmbH, Germany). Two micrograms of total RNA were primed with 50 pmol anchored-oligo $(dT)_{18}$ and transcribed with the Transcriptor First Strand cDNA Synthesis Kit (Roche Diagnostics, Germany), according to the manufacturer's protocol. Quantitative RT-PCR was performed; DNA polymerase and SYBR Green I (Finnzymes Oy, Espoo, Finland) were set in a reaction volume of 20 μL containing gene-specific primers (5 μM) and cDNA (corresponding to ~50 ng total RNA). The reaction was performed using the DNA engine Opticon 2 real-time PCR detection system (Bio-Rad Laboratories, Hercules, CA). The $2^{-\Delta\Delta CT}$ method of relative gene expression was employed and standard deviation with a ct value of <0.3 was accepted. Results are expressed as arbitrary units in comparison with the expression of GAPDH.

Primers Used for This Study

The sequence data of the genes were found with GenBank and the sequences of primers were designed with Primer3 (http://frodo.wi.mit.edu/cgi-bin/primer3/primer3_www.cgi). GAPDH was used as a housekeeping gene. The sequence and information for primers used in this study are as follows: CD36 (GenBank accession number NM_001159558): 5'-gagcaactggtggatggttt-3' and 5'-gcagaatcaagggagagcac-3', FATP-4 (NM_011989): 5'-atcaacaccaaccttaggcg-3' and 5'-aacccttgtctgggtgactg-3', FABP1 (NM_017399): 5'-catccagaaagggaaggaca-3' and 5'-ttttccccagtcatggtctc-3', FABP2 (NM_007980): 5'-ttgctgtccgagaggtttct-3' and 5'-gctttgacaaggctggagac-3', FAS (NM_007988): 5'-gctgcggaaacttcaggaaat-3' and 5'-agagacgtgtcactcctggactt-3', SCD1 (NM_009127): 5'-ccttcccccttcgactactctg-3' and 5'-gccatgcagtcgatgaagaa-3', DGAT-1 (NM_010046): 5'-gtgcacaagtggtgcatcag-3' and 5'-cagtgggatctgagccatc-3', DGAT-2 (NM_026384): 5'-agtggcaatgctatcatcatcgt-3' and 5'-aaggaataagtgggaaccagatca-3', MGAT-2 (NM_

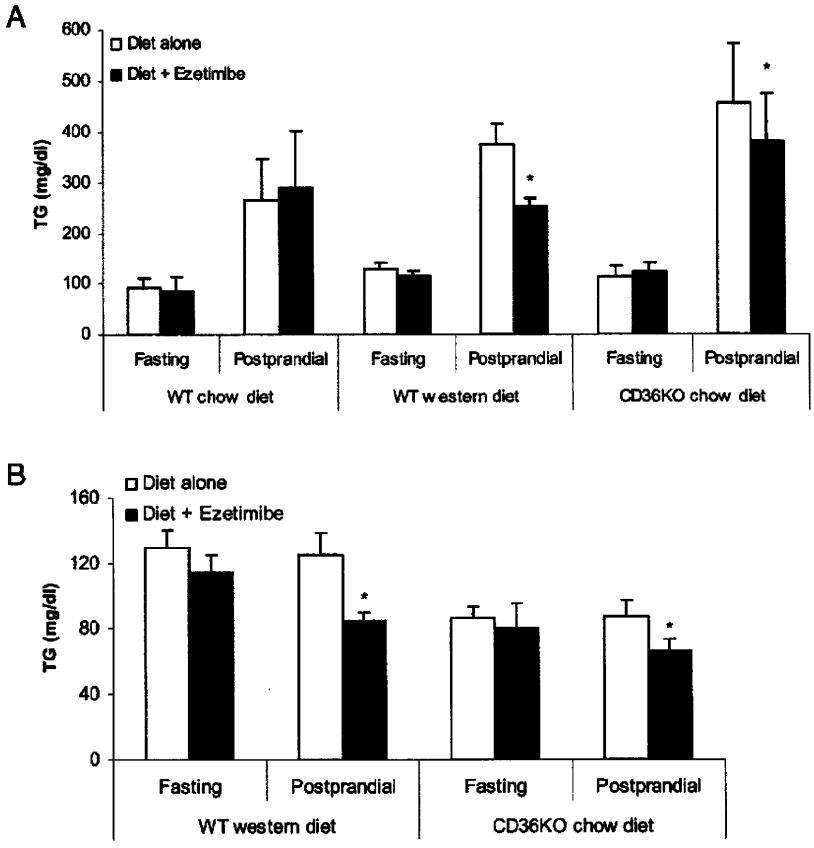

Fig. 1. Ezetimibe Reduces Postprandial Hypertriglyceridemia in Both CD36KO and WT Mice.

CD36KO mice fed a standard chow diet and WT mice fed a western diet, respectively, showed significantly higher plasma TG levels than WT fed a standard chow diet in the postprandial state (white bars) in non-treated groups. Administration of ezetimibe (black bars) decreased plasma TG concentrations at postprandial state in both CD36KO and WT fed a western diet but not in WT mice fed a standard chow diet (A). Ezetimibe also reduced the postprandial concentration of total cholesterol in plasma of both study groups (B). (*$p < 0.05$)

177448): 5'-gaagaagcagcatcagggac-3' and 5'-gtgtgggatt-agggggactt-3', ApoB (NM_009693): 5'-tgggattccatct-gccatctcgag-3' and 5'-gtagagatccatcacaggacaatg-3', Apobec1 (NM_031159): 5'-accacaacggatcagcgaaa-3' and 5'-tcatgatctggatagtcacaccg-3', ACF (NM_001081074): 5'-agccagaatcctgcaatcc-3' and 5'-agcata-cctcttcgcttcatcc-3', ACSL1(NM_007981): 5'-tgacctc-tccatgcagtcag-3' and 5'-agcctatgcactcagcgagt-3', HMGCR (NM_008255): 5'-ctggaattatgagtgccccaaa-3' and 5'-acgactgtactgaagacaaagc-3', ACAT2 (NM_009338): 5'-tgtcacagaacagggcagag-3' and 5'-tgacagttcc-tgtcccatca-3' MTTP (NM_008642): 5'-catgtcagccatcct-gtttg-3' and 5'-ctcgcgataccacagactga-3', and GAPDH (NM_008084): 5'-actccactcacggcaaattc-3' and 5'-tctc-catggtggtgaagaca-3'.

Statistical Analysis

The values were expressed as the means ± S.D. Statistical significance was assessed by Student's *t*-test for paired values and set at $p < 0.05$.

Results

Ezetimibe Reduces Postprandial Hypertriglyceridemia in Both CD36KO and Wild Type Mice

CD36KO mice fed a standard chow diet and WT mice fed a western diet showed significantly higher plasma TG levels than WT fed a standard chow diet in the postprandial state without ezetimibe treatment (CD36KO 457 ± 114 mg/dL, WT western diet 376 ± 41 mg/dL vs WT chow diet 267 ± 81 mg/dL. $n = 25$). Administration of ezetimibe decreased plasma

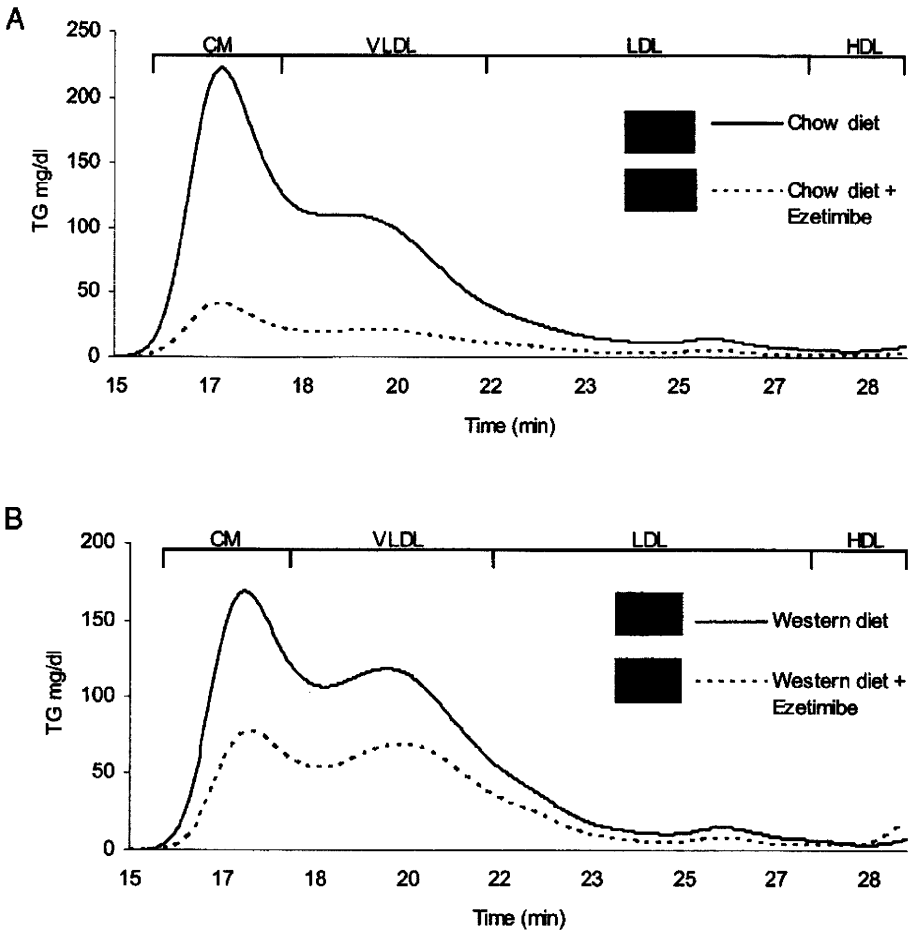

Fig. 2. Ezetimibe Reduces Postprandial CM- and VLDL-sized Particles As Well As ApoB48 Mass in Plasma of WT and CD36KO Mice.

Plasma lipoprotein profile was analyzed by HPLC. Ezetimibe (dotted line) reduced the average postprandial TG levels in both CD36KO (A) and WT mice (B) in CM- and VLDL-sized subfractions, which corresponded to CM remnants. Moreover, ezetimibe decreased the ApoB48 mass in plasma in both groups (representative sample). These results support the idea that ezetimibe might have some modulating effect on intestinal CM production.

TG concentrations in the postprandial state in both CD36KO and WT fed a western diet but not in WT mice fed a standard chow diet (**Fig. 1A**) as well as plasma total cholesterol concentrations in plasma in both study groups (**Fig. 1B**). The selective decrease in both postprandial TG levels suggests that the ezetimibe action on plasma TG concentrations is enhanced by a postprandial MetS environment, since both affected groups are indeed animal models of postprandial hyperlipidemia.

Ezetimibe Reduces Postprandial CM and VLDL-Sized Particles as Well as ApoB48 Mass in Plasma of WT and CD36KO Mice

Plasma lipoprotein profile was analyzed by HPLC using five samples for each group. The highest peak corresponded to CM- and VLDL-sized fractions in both ezetimibe-treated and non-treated mice in both groups. We found that ezetimibe reduced postprandial TG levels in both WT and CD36KO mice mainly in CM- and VLDL-sized subfractions, which corresponded to CM remnants (**Fig. 2A** and **2B**). Moreover, ezetimibe decreased the ApoB48 mass in plasma in both groups. These results support the idea that ezetimibe might have some modulating effect on intestinal CM production. Thus, we further investigated lipoproteins in the intestinal lymph, the intestinal absorption of tritium-labeled FAs, and intestinal mRNA expression of a variety of genes involved in CM synthesis in both strains of mice in the postpran-

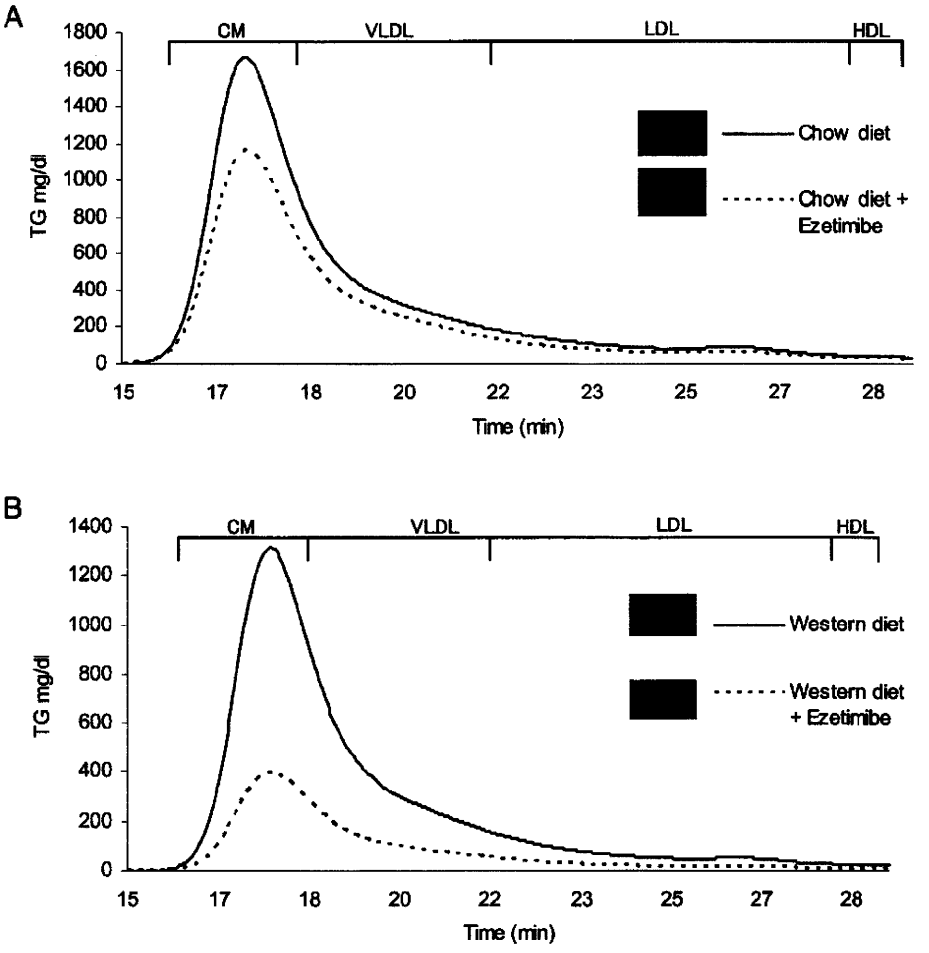

Fig. 3. Ezetimibe Reduces Postprandial TG and ApoB48 Mass in Intestinal Lymph of WT and CD36KO Mice.

HPLC analysis showed that ezetimibe (dotted lines) reduced significantly the average postprandial TG concentration in the intestinal lymph of CD36KO (A) and WT (B) mice in the postprandial state; this reduction was accompanied by a decrease in ApoB48 mass. Ezetimibe decreased the CM peak in both groups, suggesting that it might act by lowering the production of intestine-derived lipoproteins in the postprandial state.

dial state with and without ezetimibe treatment.

Ezetimibe Reduces Postprandial TG and ApoB48 Mass in Intestinal Lymph of WT and CD36KO Mice

Ezetimibe reduced the postprandial TG concentration significantly in intestinal lymph of both study groups in the postprandial state; this reduction was accompanied by a decrease in apoB48 mass in lymph. The highest peak in TG levels corresponded to the CM fraction in treated and non-treated mice in both groups. Ezetimibe decreased the CM peak, suggesting that it might act by lowering the production of intestine-derived lipoproteins in the postprandial state in both groups of mice (**Fig. 3A** and **3B**).

Ezetimibe Reduces the Intestinal Absorption of Radio-Labeled Triolein

To investigate the possible mechanisms by which ezetimibe reduced the intestinal TG secretion, we evaluated intestinal FA absorption. Ezetimibe-treated and non-treated mice from both strains were loaded with 17 μL/g olive oil containing 3 μCi of [9,10-^{3}H(N)] triolein. At 3 h after oral fat loading, ezetimibe significantly reduced ^{3}H radioactivity in the plasma of both strains (**Fig. 4A** and **4B**), establishing that there is a reduction in intestinal FA absorption associated with the administration of ezetimibe.

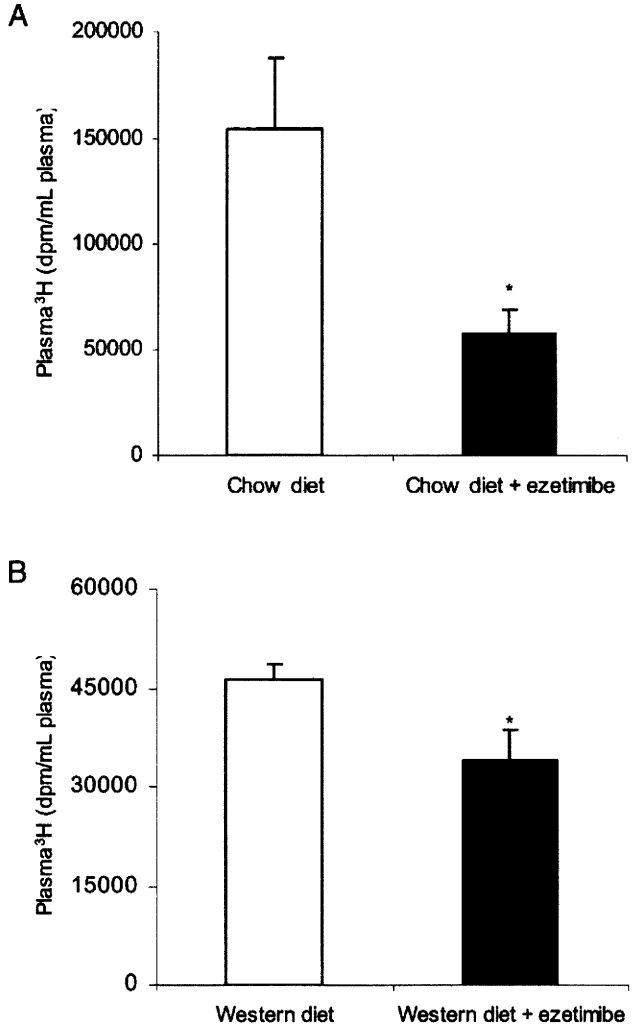

Fig. 4. Ezetimibe Reduces the Intestinal Absorption of Labeled Triolein.

Treated and non-treated mice from CD36KO (A) and WT mice (B) were loaded with 17 μL/g body weight of olive oil containing 3 μCi of [9,10-^{3}H(N)] triolein. Three hours after oral fat loading, ezetimibe reduced significantly ^{3}H radioactivity in plasma of both groups. ($^*p < 0.05$)

Effect of Ezetimibe on the Transcriptional Regulation of Genes Involved in Fatty Acid Transport, TG Formation and CM Assembly in the Intestinal Cells in the Postprandial State

To determine the molecular mechanisms involved in the attenuation of PHTG by ezetimibe, qRT-PCR using total mRNA isolated from the small intestines was performed, and the expression of genes associated with FA transport, TG formation and CM assembly in the intestine of both strains treated and non-treated with ezetimibe was examined.

In CD36KO mice, the mRNA levels of fatty acid transport protein 4 (FATP4), the only FATP in the intestine, were significantly reduced by the administration of ezetimibe, whereas the mRNA levels of fatty acid binding protein 1 (FABP1) and FABP-2, which are also associated with the transport of long-chain FAs, were not changed significantly in the treated groups. The mRNA expression of stearoyl-coenzyme A desaturase 1 (SCD1), diacyl glycerol acyl transferase 1 (DGAT1), DGAT-2, and monoacyl glycerol acyl transferase 2 (MGAT2), all involved in the intracellular formation of TG in intestinal epithelial cells, did not change significantly in the presence of ezetimibe. Interestingly, ApoB mRNA was found to be decreased in mice treated with ezetimibe; this reduction might be associated with a decrease in the expression of apobec-1 mRNA, one of the important factors and components of the protein complex involved in the mRNA edition of ApoB. The expression of microsome triglyceride transfer protein (MTP), which has an important role in CM assembly in intestinal cells, did not change significantly in the presence of ezetimibe. These results suggest that reduction in the hypertriglyceridemic response of ezetimibe in CD36KO mice might be associated with a decrease in cholesterol absorption, fatty acid transport and apo B48 synthesis, resulting in the attenuated formation of CM by a reduction of apoB48 mRNA (**Fig. 5A**).

In WT mice fed a western diet, the mRNA levels of FATP4 and FABP2 were found to be reduced by the administration of ezetimibe, while FABP1 and CD36 were unaffected by this treatment; we also found that SCD1, DGAT1 and DGAT2 were decreased in treated mice. Moreover, in this group, we also found that apoB mRNA was decreased, and this reduction might be associated with a decrease in ACF (apobec-1 complementary factor), a component of the apoB mRNA editing complex. These results suggest that ezetimibe reduces PHTG in WT mice by decreasing fatty acid transport, TG formation and CM assembly in intestinal epithelial cells (**Fig. 5B**).

We also identified an upregulation of fatty acid synthase (FAS), and acetyl-Coenzyme A acetyltransferase 2 (ACAT2) in both groups, which might be due to compensatory responses to the reduction of fatty acid transport and CM production.

Discussion

In the present study, we have investigated the inhibitory effect of ezetimibe on PHTG in MetS using two different animal models: WT mice fed a western, high fat, high cholesterol diet; and CD36KO mice, which is considered as a model of PHTG and a mono-